RETORTING POTENTIAL OF LIGNITE OVERBURDEN FROM CLAY MINING

J.C. Hower, U.M. Graham, R.F. Rathbone, and T.L. Robl

University of Kentucky
Center for Applied Energy Research,
Lexington, KY 40511-8433

Keywords: Lignite, Pyrolysis, Oil Yields

Lignite is found in the Eocene formations in the Gulf Coast Province from Texas north to Kentucky and east to Georgia. Commercial development of the lignite as an energy resource is currently confined to Texas and Louisiana where mine-mouth power plants are large consumers of lignite. The lignite in other Gulf Coast Province states is not mined as a product at the present time.

Lignite is present in the eight-county Jackson Purchase region of Kentucky at the northern end of the Mississippi embayment. The Claiborne Formation, the primary lignite-bearing formation in Kentucky, is dominated by clay deposits with associated lignites and sands. The lignite and clay bodies were deposited as narrow elongate deposits, which resulted from the filling of oxbow lakes over periods of 500 to 1500 years. The axis of the fluvial depositional system migrated east then back to the west over the course of the Claiborne deposition.

The lignite sample was obtained from the Eocene Claiborne Formation, Milburn 7½ minute quadrangle, Carlisle County, Kentucky. Lignite is removed as overburden in the mining of ball clay from the Eocene of Kentucky's Jackson Purchase region, but is not currently mined as an energy resource but rather is a waste product. About 160 kt of clay was mined in 1991 (Kentucky Department of Mines and Minerals) with an estimated 40 kt of lignite moved in the process. The high moisture, low heating value lignite has not been competitive as an energy resource due to its proximity to the higher quality bituminous coals in the nearby Illinois Basin and, more recently, to the import of Powder River Basin coals into the lower Ohio River Valley. In this study, we examine potential uses of the lignite which could provide the opportunity to develop it as an added resource along with the clay.

Results and Discussion

Petrography of the Lignite

The petrography of the lignite is rather typical of other lignites from the region in having a high percentage of detrital macerals: humodetrinite and liptodetrinite (Table 1). Petrographic analysis of those macerals is difficult owing to their fine (generally less than 10 μm) size and consequent difficulty of resolution in either white-light or blue-light microscopy. Blue-light excitation is an aid in resolving some liptinite macerals in complex mixes. Liptinite macerals

in this and other Kentucky lignite samples evolve mobile constituents in the form of the maceral fluorinite. The reflectance of lignite is typically measured on ulminite. The low percentage of ulminite in this lignite limited the number of measurements. Ulminite reflectance was determined to be 0.21%, consistent with previous samples from the same mine. The petrology of the Eocene lignites in the Jackson Purchase region was discussed by Hower et al. (1990).

Pyrolysis of the Lignite Sample

The lignite sample was retorted in N_2-swept fixed bed experiments. The production of oil from a waste overburden, such as the present lignite, would make the economics of clay mining in this region even more attractive. Accordingly, the lignite sample was first ground to a grain size of 18 x 20 mesh and fed into a retort to establish the lignite's oil yield potential. The N_2-swept fixed bed experiments were performed in a 1.5 inch stainless steel reactor. Oil vapors and sweep gas passed through a 100 micron filter at the base of the reactor. Heating rate was 4° C/minute with a maximum bed temperature of 550 °C. The reactor conditions are discussed in detail by Rubel and Coburn (1981). The objective of this part of the research was to obtain the oil yields of the lignite sample. Results of the retorting experiments indicate that 11.7 wt % oil may be obtained during pyrolysis.

The oils derived from the lignite are very waxy. Large amounts of water were also captured during the retorting of the lignite sample. Because most of the water was released before the sample was heated to above 150 °C it may be concluded that only small amounts of structural water were released by clay minerals which occur as ash components within the lignite sample.

The processed lignite sample was analyzed for carbon, hydrogen, nitrogen, and sulfur using automated LECO elemental analyzers. Ultimate and proximate analyses of the retorted lignite sample are illustrated in Table 2. The majority of the moisture was released during pyrolysis. After pyrolysis the retorted lignite sample was found to have very high fixed carbon values [Table 2].

Heating Stage Microscopic Examination of the Lignite Sample.

The heating stage microscope (HSM) apparatus utilized in this study consists of a Zeiss Universal polarized light microscope, a heating stage, and temperature and gas flow controllers. A polished shale sample was positioned in the heating chamber and could be observed at any time using a polarized light microscope. The sample chamber consists of three quartz plates which help to channel the preheated N_2-gas flow above and below the sample for optimum temperature control. The hot stage was equipped with a monitor and video camera for real time observations. Most importantly, the HSM -apparatus allowed the *in situ* observation of the pyrolysis process of the lignite sample.
Because the HSM-study permitted the use of larger lignite particles than those used in the reactor, the retorted parts were big enough to preserve the spatial relationships between the charred macerals, mineral matter and macro-pores that were generated during oil evolution.

Observations of the process induced macroporosity in the retorted (spent) lignite sample were made possible using a scanning electron microscope (SEM; Hitachi 2700-S), which allowed a magnification of the sample by $x10^4$ times. Structural changes in the retorted lignite sample are documented in Figure 1 and Figure 2. The SEM results indicate that volatilization of macerals causes a complex network of macropores to develop which typically have the shape and size of the macerals in the raw lignite. A multitude of cracks also formed throughout the lignite sample (Figure 1), which probably aid in the escape of the oil vapors. Prior to pyrolysis, cracks were not observed in the lignite sample (Figure 1).

Not all of the macerals contribute to the oil phase when heated in the retort. The pyrolysis residue was primarily composed of uniformly reflecting isotropic semi-coke and unreacted inertinite macerals, primarily sclerotinite. Semi-coke with the texture of the huminite maceral textinite was observed. Other huminite macerals, and perhaps a portion of the liptinite component, are preserved as a porous semi-coke with little preservation of the original morphology. Anisotropic semi-coke, perhaps as a retrograde product of evolved liquids, was a rare component. Pyrrhotite was observed, but silicates are the more common mineral form in the residue.

Summary and Conclusions

Lignite is presently removed as overburden in the mining of ball clay in the eight-county Jackson Purchase region of Kentucky rather than mined as an energy resource. Although this is mainly due to the fact that higher quality bituminous coals are mined locally, the removal of the lignite causes both environmental and economical concerns. This lead to the objective of this study to examine potential uses of the lignite to be utilized as an added resource along with the clay. Liquid product recovery after pyrolysis of the lignite indicates that this waste product contains 11.7 wt % of oil. Furthermore, a carbon-rich solid remains after pyrolysis. Upon retorting the lignite was observed to have formed an intricate network consisting of variously sized pores and charred carbonaceous material. Heating stage microscope (HSM) observations helped to establish the spatial relationships between process induced pores and char. In addition, the HSM-experiments allowed the precise determination of the boiling temperature when constituents in the macerals start to vaporize. The development of a porous structure in the carbon-rich pyrolysis residue of the lignite under investigation may indicate the lignite's potential as source material for the production of adsorbent carbons. Utilization of the lignite in the production of liquid fuels, and possibly as carbon precursor, may help in the regulation of a waste material.

Acknowledgements The Authors would like to thank G. Thomas, M. Moore, and M. Spears for analytical and technical support.

References

1 Hower, J.C., Rich, F.J., Williams, D.A., Bland, A.E., and Fiene, F.L., 1990, Cretaceous and Eocene lignites, Jackson Purchase, Kentucky: Int. Journal of Coal Geology, v. 16, p. 239-254.

2 Rubel, A.M. and Coburn, T.T., 1981, Eastern Oil Shale Symposium, Kentucky Energy Cabinet, Lexington, KY, p. 21

Table 1 Maceral Composition of the Lignite

Maceral	Sample 91999 (W. KY)
Textinite	0.7
Ulminite	3.5
Humodetrinite	35.1
Gelinite	0.4
Corpohuminite	5.5
Fusinite	3.3
Semifusinite	0.3
Sclerotinite	1.1
Inertodetrinite	0
Exinite	6.3
Resinite	2.3
Suberinite	1.6
Liptodetrinite	39.1
Alginite	0.8

Table 2 Ultimate and Proximate Analyses of Raw and Pyrolyzed Lignite Sample

	91999	91999	91999	91999p	91999p	91999p
	as rec.	dry	daf	as rec.	dry	daf
Moisture	10.97					
Ash	19.11	21.16		3.21		
Volatile Matter	51.30	57.62	73.36	35.53	36.71	
Fixed Carbon	18.60	20.89	26.64	21.64	22.36	35.33
Carbon	50.00	56.16	71.50	39.60	40.91	64.67
Hydrogen	6.03	5.39	6.86	56.11	57.97	91.59
Nitrogen	0.96	1.08	1.37	2.15	1.85	2.92
Oxygen	11.85	14.70	18.73	1.07	1.11	1.75
Sulfur	1.08	1.21	1.54	0.52	0.90	1.43
Heating value (Btu/lb)	8690			1.41	1.46	2.31
Heating value (MJ/kg)	20.26					

91999 = lignite raw sample 91999p = pyrolyzed lignite sample

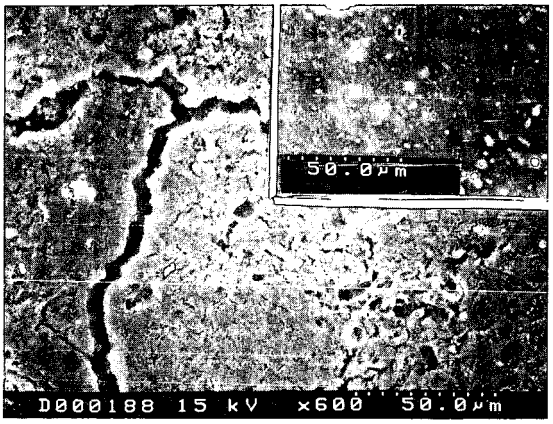

Figure 1 SEM-microphotograph of a polished section of the lignite sample. The insert presents the raw lignite sample before the heating stage microscope (HSM) experiment. The polished lignite surface shows only minimal signs of cracks or pores. The main photo shows the surface of the lignite sample after pyrolysis in the HSM. The surface is characterized by abundant cracks of various sizes and large amounts of elongated macropores.

Figure 2 Magnification of lignite sample shown in SEM-microphotograph of Figure 1. Macropores develop during pyrolysis. The spatial relationship among macropores, and that of the macrostructure stabilizing char and mineral matter are preserved during the HSM experiments.

Fractionation of Coal Extracts with Bacterial Enzymes.

Leonard L. Matz
Matz & Associates
3061 Bishop Road
Appleton, NY 14008

ABSTRACT: Common and novel bacterial enzymes or *de novo* synthesized unique organic ethers reacted with Coal extracts yielding coal breakdown products. The diphenyl ether was synthesized *de novo* from methyl benzoate and 1-Diphenyl-1,3-butanedione preparation of the di-cation of butanedione with the aid of sodium hydride (NaH). After synthesis of 2,6-Diphenyl-4-methoxypyridine and other less common ethers, dissolution of coal fractions yielded various levels of carbon fragments. Ether extraction of Coal (Illinois No. 6) resulted in release of aromatic and short chain fractions. Enzymatic dissolution of Coal and ether extracts also yielded identifiable carbon fragments. Specific enzymatic dissolution of Coal with pure flavin containing enzymes remains a goal. This approach involves: 1-more complete kinetic characterization of the proposed NADPH Reductase/comproportionation system, 2-initial experimentation into flavodoxin components common to both the Nitrogenase system and the electron transport system of *Azotobacter vinelandii*, 3-the degree of complementarity between these systems judged by component interaction and immunologic cross reactivity.

INTRODUCTION: *De novo* synthesized ethers reacted with Coal Extracts yielding breakdown products (1). A novel pyridine ether (I) synthesized *de novo* from 1-Phenyl-1,3-butanedione and methyl benzoate and two more common pyridine ethers (II & III) solubolized dried Coal Extracts (Fig.1).

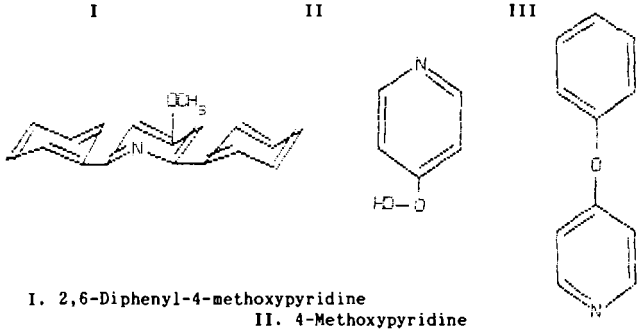

I. 2,6-Diphenyl-4-methoxypyridine
II. 4-Methoxypyridine
III. 4-Phenoxypyridine

Fig 1. Organic Structures

The purpose of these experiments, in general, is to differentiate the ultrastructure from that of living structure such as the bacterial spore. In particular, unlike bacterial spores that possess easily discernible pore sizes, coal is much more difficult to approximate because of its local regions of heterogeniety. That is unlike bacterial spores, different regions of the coal ultrastructure apparently differ markedly from other domains of the ultrastructure. Interaction of the pyridine ethers with the coal structure can considerably curtail interpretation. However, the study reported above

describing the abbreviated exposure of 4-methoxypyridine pyridine to coal assumes limited if not exclusionary chemical reaction with the coal. The ultrastructure of coals is susceptible to study using small molecular weight organic molecules that are not susceptible to alternation by the interior of the coal pores. In these experiments commonly accepted organic molecules that are very resistant to alternation in such organic milieu, ethers. Theoretically these molecules can be used as molecular sieves to approximate the size of coal pores. Unfortunately, the pyridine ethers are somewhat unreasonable solvent because they react with the coal ultrastructure after prolonged periods of time. Generally, however, the ethers and the enzymes reactions with the coal were understandable and provided valuable data.

RESULTS:

1,5-Diphenyl-1,3,5-pentanetrione 1,5-Diphenyl-1,3,5-pentanetrione, the enolate carbanion of 1-phenyl-1,3-butanedione, formed after proton extraction with sodium hydride in the aprotic solvent, 1,2-dimethoxy ethane (monoglyme). Condensation of this carbanion with methyl benzoate yielded the triketone, 1,5-diphenyl-1,3,5-pentanetrione. This aroylation apparently involves the di-anion of the B-diketone which forms in a

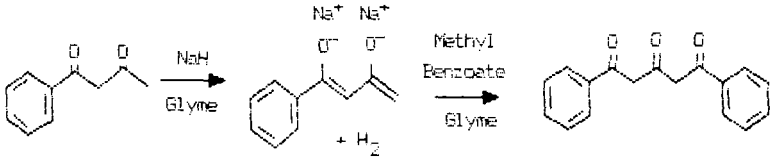

Fig. 2. Synthesis of 1,5-Diphenyl-1,3,5-pentanetrione

"step-wise" extraction of its a-hydrogens. The terminal a-hydrogen is not the first extracted from the b-diketone, but is only extracted after mono-anion formation and in the presence of methyl benzoate. The terminal a-hydrogen is, however, the site of reaction of the b-diketone with the carbonyl carbon of the ester. The methoxide group of the ester, neutralized by the Na+ counter ions, then leaves the condensation product. Exposure to air with its incipient moisture and neutralization of the reaction mixture with 6N HCl provide the protons for neutralization of the carbanions present and formation of the triketone.

This reaction occurs with a high degree of efficiency yielding 80-90% product (86.9%). Apparently once formed, the di-anion is quite reactive and the reaction is evidently highly selective for the terminal carbon of the dianion. As expected, the symmetric triketone formed, was soluble in diethyl ether, but its solubility varied considerably depending on the pH of the reaction mixture.

These differences could be a reflection of minor changes in the structure of the triketone. The spectral data substantiates that they are not reflective of impurities present. Variation of the color, crystalline form and melting points of the triketone which substantiate similar earlier observations are also suggestive of small variations in the structure of the triketone. Because of the H-bonding, various keto-enol tautomeric forms can be envisioned and as pH changes occur in the solvent all of these forms are undoubtedly present in the solution. At low pH values the triketone is probably found as a doubly H-bonded enolic structure (Formula 4), at intermediate pH values as a mono-H-bonded structure (Formula 2) and at high pH values as a keto form (Formula 1) with little H-bonding.

2,6-Diphenyl-4H-pyran-4-one The triketone can be protonated in concentrated sulfuric acid in the 1-or 5-keto position leading to the formation of enolic

triketones. The triketone is then cyclized by the formation of an intramolecular acetal. Upon dehydration the pyran is completed yielding the 2,6-

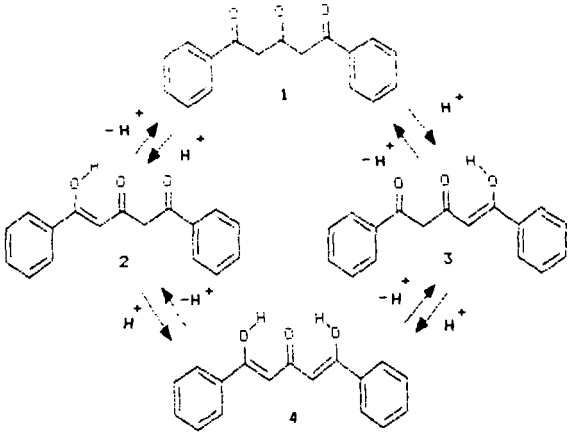

Fig. 3. Hydrogen Bonding of 1,5-Diphenyl-1,3,5-pentanetrione

diphenyl-4H-pyran-4-one. The reaction occurs with great efficiency (89-91%) suggesting that the stability of the 6-membered ring in the product is the selecting factor in the formation of the pyran derivative.

2,6-Diphenyl-4(1H)-pyridinone This pyridinone was produced by the cyclization of the 1,5-diphenyl-1,3,5-pentanetrione with liquid ammonia. Because of the high pH of the reaction milieu, which causes the enolization of the ketone groups, the addition product is the primary amine-enol or dienol intermediate.

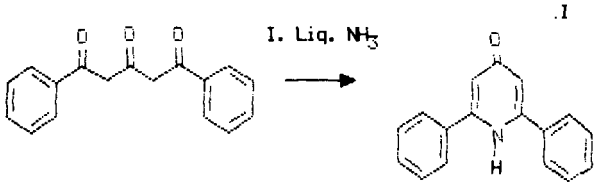

Fig. 4. Synthesis of 2,6-Diphenyl-4(H)-pyridinone

Cyclization by addition of the primary amine to the other terminal carbon of the pentanetrione chain then readily occurs (Table 1).

This di- or trienolic structure is then dehydrated to form the highly conjugated diphenyl-pyridine derivative with its quinoid-like pyridine ring. Noteworthy in this synthesis is the modification of the original synthetic procedure by addition of the dehydrating agent, sodium sulfate, to the reaction milieu. The combination of the anhydrous ethanol and sodium sulfate promoted the reversible dehydration of the product and gave an increase in yields of 32.3-35.4 to 66.6-75.1%.

Table 1. Physical Properties of Synthetically Prepared Precursors and Ethers

This addition had little effect on the physical properties of the product. The yields were also increased from a literature value of 45% to an average value of 70% in our experiments. Also, sodium sulfate added in only the second step was equally effective. In the presence of this additional dehydrating agent, the efficiency of the reaction is quite high. Because the product pyridinone is highly conjugated investigators have obtained its UV spectrum. This property and the electronic configuration around the heterocyclic nitrogen, suggest that the molecule may be

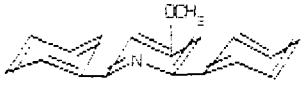

Fig. 5. 2,6-Diphenyl-4-Methoxypyridine (A)

planar even though this would involve an eclipsed conformation of the phenyl rings (A) and the pyridinone. Steric hindrance would not preclude this possibility, since the phenyl rings could move freely about the carbon to connecting them to the heterocyclic ring. The heterocyclic ring is of a quinoid not benzenoid configuration which disallows enol formation of the keto group in the C-4 position. The highly conjugated nature of the pyridinone allows little stereochemical analysis of the molecule which contains no asymmetric carbon, but the presence of two chiral centers during the closure-dehydration mechanism suggests specificity of the protons lost from the C-3 and C-5 positions as dehydration occurs. The formation of the double peak feature at 3090 and 3140 cm-1 not found in the original triketone, is evidence of the presence of the heterocyclic This coincides with the loss of some of the carbonyl intensity and features. This is also strongly suggested by the loss of IR features from 900-1299 cm-1. The NMR spectrum also reveals the downfield migration of the non-aromatic protons of the triketone to the C-3 and C-5 protons of the heterocyclic ring. The signal for these protons occurred within the signal for the three terminal protons of each phenyl ring of the pyridinone. It could be observed when using a sweep width of 250 instead of 500 Hz. The proton of the heterocyclic nitrogen was not observable even at a chemical shift of 15 ppm. Mass spectral analysis revealed a molecular peak at 247 me units and the usual fragments associated with the molecule. The synthesized pyridinone possessed the literature values of the physical properties. In addition, the physical properties of the triketone and pyran were considerably different. These results suggest because of their interdependence that the structural parameters attributed to these isolates are consistent and reputable.

Enzymatic Properties

Enzymological Purification of NADPH:Flavodoxin Oxidoreductase Ten to fifteen mgs of purified reductase remained after purification of 220 times from the 250,000 x g supernatant. Gel filtration of the FLD reductase succeeds only on large diameter pore size gels, i.e., Sepharose 2B or 4B or Ultragel-32. This suggests either a very large molecular weight enzyme, complexation of the enzyme with other proteins, or polymerization of a small molecular weight enzyme into large aggregates. Spectra of the flavin group of the enzyme undergo reduction by light and EDTA. The absorption spectrum of Flavodoxin Oxidoreductase that contains a FAD residue as a prosthetic group is sensitive to EDTA reduction in light.

Enzymological Properties Purified FLD reductase shows little selectivity of substrates and reaction rates appear entirely dependent on the redox potential of the substrate. Progress curves of $FLDH_2$ formation are biphasic and suggest an initial rapid rate of $FLDH_2$ formation (0-2 ms) and a second more persistent $FLDH_2$ formation (2-12 ms) (Table 2). Double reciprocal plots of either rates are straight lines over a limited range of substrates concentration (15-50 mM FLD_{Av}). The initial rate of formation of $FLDH_2$ resides within the reduction rate range described for the other electron acceptors. The Km of $FLDH_2$ formation is also quite comparable to that of the other electron acceptors (Table 2). The change of K_m at 2 ms

Table 2. Enzyme Parameters and Kinetic Constants of the Enzymatic Reduction/Comproportionation of FLD_{Av} and the Me-FLD_{Av}.

of K_m at 2 ms is consistent with the idea that the affinity of the FLD for the FLD reductase changes as the $FLDH^*$ concentration increases. If this is the operative mechanism of FLD_{Av} reduction that is quite consistent with the fluorescent data, it suggests that NADH reduces FLD then the $FLDH_2$-NAD^+ complex reduces FLD_{Av}.

Enzymological Reactivity

Spectrophotometric Assay: The enzymatic reduction of both FLD and N_3-CH_3-FLD straight forwardly demonstrates the primary formation of $FLDH^*$ and its analogue. The initial velocity (v_0) was 10% larger for substituted flavodoxin indicating that it is a better substrate. The formation of N_3-CH_3-$FLDH^*$ also remains more sustained producing 32% of the possible N_3-CH_3-$FLDH^*$ in the first 10 ms of reduction. During the same period 16% $FLDH^*$ undergoes reduction. Second order rate equations facilitated quantitation of these kinetic differences.

Product Formed Graphic representation of the hydroquinone formation (Reaction 1) exhibits a shift from one constant (k_{1a}) to another (k_{2a}) as the reaction proceeds. The duration of the initial kinetic parameters varies greatly from native to substituted flavodoxin. The modification of the initial rate (slope) occurs more quickly and completely with FLD. This modification accelerated by ionic strength, causes further displacement of the 5 mM Tes, line toward the x-axis at 25 mM Tes. Contrariwise, these ionic strengths don't affect the secondary kinetic constants because the slopes remain constant. The dFLDH*/dti is about as large at 25 mM Tes. Its formation is linear throughout the observed reduction.

Enzymological Properties of NADH:Ferricyanide Dehydrogenase: Topological and ultrastructural membrane features accrued during comparison of walled, *Staphylococcus aureus*, and wall-less, *Acholeplasma laidlawii*, bacterial membranes. Osmotic lysis of protoplasts of these organisms produced membrane vesicles or large membrane fragments, but alumina grinding or sonication of these protoplasts or cells produced much smaller particles whose morphologic origin was difficult to determine. Disrupted membranes from either organism were covered with ribosomes from 15 to 30 nm diameter adhering almost exclusively to the inside of the vesicles or fragments.

An NADH dehydrogenase possessing a specific activity 3-5 times that of membrane bound enzymes was obtained by extraction of *A. laidlawii* membranes with 9.0% ethanol at 43° C. This dehydrogenase contained only trace amounts of iron (suggesting an uncoupled respiration), a flavin ratio of 1:2 FAD to FMN, and 30-40% lipid, which could explain its resistance to sedimentation. It efficiently utilized ferricyanide, menadione and dichlorophenol indophenol as electron acceptors, but not O_2, ubiquinone Q10 or cytochrome c. Lineweaver-Burke plots of the dehydrogenase were altered to linear plots of the dehydrogenase were altered to linear functions upon extraction with 9% ethanol. In comparison to other respiratory chain-linked NADH dehydrogenases in cytochrome containing respiratory chains, this dehydrogenase was characterized by similar K_m's with ferricyanide, dichlorophenol indophenol, menadione as electron acceptors, but considerably smaller V_{max}'s with ferricyanide, dichlorophenol indophenol, menadione as electron acceptors, and smaller specific activities. Some kinetic properties of the dehydrogenation, the uniquely high glycolipid content and apparently uncoupled respiration at Site I characterized this NADH dehydrogenase from this truncated respiratory chain.

DISCUSSION:

Studies revealed hydrogen bond activation of alkyl-aryl ethers (I) toward cleavage by formation of its mono- then di-anion and combination with methyl-benzoate. These reactions provide good yields due to the driving force of the charged molecular species. Our yields provide excellent conditions for continued synthesis of ether precursors. Unfortunately, the inefficiency of the diphenyl-chloropyridine and the phenyl-ether synthetic steps limited the total yields of ethers.

Current thinking now suggests that coal is an elastomer in which strong internal hydrogen bonding gives it high internal glass transition temperatures. The same acidic hydrogen donors and basic hydrogen receptors that provide strong hydrogen bonds in the bulk structure populate the surface of coal powders. A dominant property of this molecule is the H-bonding capacity of the 2,6-diphenyl-1,3,5-pentanetrione. A variety of physical properties reflected this dominating molecular effect during isolation procedures.

REFERENCES:

1. Matz, L. L. & Buchanan, D. H. Synthesis and Characterization of Pyridine and 2,6-Diphenylpyridine Ethers, *C&E News*, 1990, 69, 69.
2. Ryan, M. D., Noker, P. E. & Matz L. L. Immunologic Properties of Glycolipids from Membranes of *Acholeplasma laidlawii*. Infect. Immun. 1976, *12*, 799.
3. Weiner, D. W. & Matz, L. L. Topologic and Ultrastructural Features of Membrane from *Acholeplasma laidlawii*. Microbios 1976, *15*, 7.
4. Jinks, D. C. & Matz, L. L. Purification of the Reduced Nicotinamide Adenine Dinucleotide Dehydrogenase from Membranes of *Acholeplasma laidlawii*, Biochim. Biophys. Acta. 1976, *452*, 3041.
5. Matz, L. L. *NADPH Dehydrogenases of Terminal Electron Transport Systems, Emerging Technologies for Hazardous Waste Management*; Tedder, W. D., Ed; Hazardous Waste Mansgement; ACS Press, Washington, D.C., 1993, 2, pp .
6. Matz, L. L. *Flavodoxin Hydroquinone-(1,5-Dihydroflavin)-as the Energy Source for Biological Nitrogen Fixation by Azotobacter vinelandii*; Himmel, M. E., Overend, R. P. & Baker, J. O., Ed.; Bioconversion for Fuels; ACS Press: Washington, D.C., 1994, 1; pp .

SUMMARY:
1,5-Diphenyl-1,3,5-pentanetrione was cyclized to form 2,6-Diphenyl-4(1H)-pyridinone with liquid ammonia. The resulting ether, 2,6-Diphenyl-4-methoxypyridine, from substitution of the keto (C-4 position) of the pyridinone, was used to extract Coal. Several extraction treatments of Coal based upon enzymatic treatment of extracted coal are foreseen.

Table 1. Physical Properties of Synthetically Prepared Precursors and Ethers

Name	Recrystallization Solvent	Color	Mp (Bp)	% Yd
1,5-Diphenyl-1,3,5-pentanetrione	95% Ethanol	Yellow	107-109	57.7
2,6-Diphenyl-4(1H)-pyridinone	Benzene	Cream	176-179	66.6
2,6-Diphenyl-4-chloropyridine	95% Ethanol	White	83-84	86.3
2,6-Diphenyl-4-methoxypyridine	Methanol	White	79-80	46.3
4-Methoxypyridine	Distilled Water	Clear	41-45	
4-Phenoxypyridine	Distilled Water	Clear	78-79	

Table 2. Enzyme Parameters and Kinetic Constants of the Enzymatic Reduction/Comproportionation of FLD_{Av} and the Me-FLD_{Av}.

Properties	FLDH		N_5-CH_3-FLDH	
	5 mM Tes pH=7.4	25 mM Tes pH=7.4	5 mM Tes pH=7.4	50 mM Tris pH=9.5
$(FLDH^{\cdot}/FLDH_2)$ of Final Product	$\frac{10.55_{\mu M}}{4.06}$	$\frac{12.75}{1.70}$		
$dFLDH_2/dt_i=v_o$	0.53 nmol	0.33	0.58	0.26
$dFLDH^{\cdot}/dt_i$	0.10	0.15	0.58	0.26
k_{1a}	$8.58 M^{-1}sec^{-1}$	5.86	8.04	2.89
k_{1b}	$2.75 M^{-1}sec^{-1}$	1.94	3.34	1.52
k_2*	$60.60 M^{-1}sec^{-1}$	318.00	31.37	30.00
K_{sq}	$0.10 M^{-1}sec^{-1}$	1.60	0.39	0.34

APPLICATION OF SELECTIVE LEACHING TECHNIQUE FOR MAJOR, MINOR, AND TRACE ELEMENT ANALYSIS IN COAL

Catherine O'Keefe, Kurt Eylands, and Debra Pflughoeft-Hassett
Energy & Environmental Research Center
University of North Dakota
Grand Forks, North Dakota 58202

Keywords: selective leaching technique

INTRODUCTION

The abundance and association of major, minor, and trace inorganic constituents in coal must be determined to predict their fate during combustion and gasification. In addition, the inorganic composition of coal influences the properties of the ash produced that, in turn, affects the usability of ash. The adverse effects of the inorganic components (ash-forming species) on coal utilization system performance include the formation of fine particulate that is difficult to collect, ash fouling and slagging, and conversion and erosion. Recently, selected metals that are present in coal were identified as air toxics. The 1990 Amendments to the Clean Air Act identified 189 hazardous air pollutants, including many trace metals. Therefore, the fate of trace metals considered to be air toxics is increasing in importance. Knowledge of the abundance and association of inorganic constituents is necessary in predicting the inorganic species behavior in coal in a given process. Chemical fractionation, in combination with other analytical techniques such as computer-controlled scanning electron microscopy (CCSEM), is used in models to predict the formation and ash deposition properties.

The inorganic components in the higher-rank coals (anthracite and bituminous) are primarily present in mineral phases. Whereas, the inorganic components in low-rank coals can be associated as discrete mineral phases, coordinated metal ions, and cations bound to carboxyl groups or in clays (1). The major mineral phases found in coal include aluminosilicates, carbonates, sulfides, and sulfates. Much of the Si, Al, and K is found in the aluminosilicate minerals such as clay minerals, with Si also found in quartz. Clays may also adsorb some trace elements such as Cs, Li, and Rb. Sulfide minerals such as pyrite can contain the trace elements arsenic, cadmium, cobalt, chromium, copper, mercury, manganese, molybdenum, nickel, lead, and selenium (2, 3). Carbonate minerals such as calcite, siderite, dolomite, and ankerite contain magnesium, calcium, and iron, but may also have trace amounts of manganese, strontium, and barium present.

The organic coal portion of coal consists of carboxylic acid, phenolic hydroxyl, mercapto, and imino groups which are able to bond with several trace elements. Cations of sodium, calcium, magnesium, potassium, barium, iron, manganese, strontium, and zinc bond to the carboxyl group to produce carboxylate salts (3). The trace elements are generally associated with both the organic and the mineral matter. In the mineral portion of coal, the trace elements can be found as discrete minor minerals, as replacement ions in minerals, or adsorbed on clays (2).

This paper discusses the application of a selective leaching technique known as chemical fractionation to coal. The method described is a modification of a leaching method by Miller and Given (4). Chemical fractionation is used to determine the distribution of elements among the organic and mineral phases in coal based on the differences in solubilities of coal constituents in three separate, stirred solutions: deionized water, 1 M ammonium acetate (NH_4OAc), and 1 M hydrochloric acid (HCl) as shown in Figure 1. A representative 140-gram sample of coal is ground to -200 mesh (< 74 micrometers) and then vacuum dried to a constant weight. A 35-gram portion of coal is ashed at 750°C and the ash content is determined. A sample is analyzed for the major, minor, and trace elements. The remainder of the coal is then subjected to successive extraction treatments. The first extraction treatment uses 4 mL of deionized water per gram of coal and is stirred in a covered beaker at room temperature for 24 hours. The sample is vacuum-filtered and

rinsed with deionized water. About 35 grams of the coal residue is removed and dried for ash content determination, and an analysis on the ash for the major, minor, and trace elements is performed by energy-dispersive x-ray fluorescence (EDXRF) utilizing direct excitation and three secondary excitation conditions (aluminum, titanium, and germanium). The filtrate is then acidified and transferred to a 125-mL volumetric flask, made up to volume, and stored for further analysis by inductively coupled plasma emission spectroscopy (ICP) and atomic absorption (AA).

Four mL of 1 M NH_4OAc per gram of coal is then added to the beaker containing the remaining 70 grams of coal residue. The sample is stirred and heated at 70°C for 24 hours. The sample is then vacuum-filtered and rinsed with deionized water. The filtrate is acidified and saved. The 1 M NH_4OAc extraction procedure is repeated two additional times. The filtrates from the three successive NH_4OAc extractions are combined, transferred to a 500-mL volumetric flask, made up to volume, and stored for analysis by AA. About 35 grams of residue coal is removed and dried. The residue coal is used for determination of the ash content, and major, minor, and trace constituents are determined on the ash by EDXRF.

To the remaining coal residue, 4 mL of 1 M HCl per gram of coal is added, stirred, and heated at 70°C for 24 hours. The sample is vacuum-filtered and rinsed with deionized water. The filtrate is acidified and saved. The 1 M HCl extraction procedure is repeated once more. The filtrate from both HCl extractions is combined, transferred to a 300-mL volumetric flask, made up to volume, and stored for analysis by AA. The coal residue is then dried. A portion of the dried coal residue is used for ash content determination, and the remainder is ashed and analyzed by EDXRF for the major, minor, and trace elements.

RESULTS AND DISCUSSION

The chemical fractionation procedure uses deionized water to extract the water-soluble minerals, such as halite (NaCl) and thenardite (Na_2SO_4). The cations associated on ionic exchange sites of carboxylic acids in the organic portion of coal are removed by ammonium acetate. Hydrochloric acid extracts elements that are associated with acid-soluble minerals, such as calcite ($CaCO_3$), dolomite ($CaMg[CO_3]_2$), and siderite ($FeCO_3$), and organic coordination complexes. The elemental constituents remaining in the residue presumably are associated with the insoluble minerals, such as clays (aluminosilicates), quartz (SiO_2), and pyrite (FeS_2).

Table 1 summarizes the chemical fractionation results obtained from five coals ranging in rank from lignite to bituminous. The ash produced by ashing (at 750°C) the chemical fractionation residues was analyzed using a Fisons 770 EDXRF system, and the mass balance was completed by normalizing to zero silicon loss. The results indicate that sodium is the only element that is consistently and appreciably extracted in the water treatment. The sodium is probably present in the coals as sodium chloride (halite), and sodium sulfate (thenardite), and, in the Beulah coal, may be present in the water inherent in the lignite.

Calcium, magnesium, and sodium in all five coals, along with some potassium in two of the coals, are removed primarily in the ammonium acetate extraction. These elements are usually found in salts of organic acids in coals. They may also be found in minerals such as gypsum which is soluble in both water and ammonium acetate, or they may be associated with ion-exchange sites in clays.

The hydrochloric acid leaching extracted a majority of the iron and aluminum that was removed during the chemical fractionation process. Much of the remainder of the calcium and magnesium that was left after the ammonium acetate leaching was removed by the hydrochloric acid extraction. These elements were probably associated with the carbonate minerals calcite and dolomite which are acid-soluble. A small amount of titanium in two of the coals was also leached out of the coal during the hydrochloric acid extraction. The hydrochloric acid extraction removes elements that exist in organic coordination complexes such as Al^{3+} and Fe^{3+} and in acid-soluble minerals such as carbonates.

The bituminous coals differed from the lignite and subbituminous coals in that less sodium and magnesium were extracted, indicating an association of sodium with the insoluble mineral fraction of the coal. A larger portion of the aluminum remains in the bituminous coals than in the lignite or subbituminous coals, suggesting that the aluminum is not associated with a coordinate site, or that there is a better developed crystalline structure of the clays such as illite and montmorillonite.

The iron in all of the coals is located in the acid-soluble or the insoluble fractions. Computer-controlled scanning electron microscopy (CCSEM) analysis of the coals indicates the percent of pyrite to be as follows: Beulah - 30%, Black Thunder - 11%, Rochelle - 2%, Illinois No. 6 - 36%, and Pittsburgh No. 8 - 13%. This indicates a direct relationship between the pyrite content and the iron content after leaching. The iron leached by HCl can be attributed to the dissolution of siderite ($FeCO_3$). This is the most evident in the Rochelle subbituminous coal.

The weathering of Pittsburgh No. 8 has caused some minerals such as pyrite to oxidize. Therefore, the oxidized iron was removed in the hydrochloric leaching, but aluminum was not because aluminum is not readily oxidized. The aluminum was removed in the lignite and bituminous coals, due to aluminum being organically associated.

Arsenic and mercury, according to Norton and others (5) and Ciocco and others (6), are strongly associated with pyrite and other sulfide minerals. Finkelman (7) and Galbreath and others (8) also have indicated that mercury is present in coal as a sulfide. Chromium is reported to be associated with clay minerals (9). Table 2 indicates that arsenic is primarily removed by hydrochloric acid, while only a small portion of chromium is removed. However, the majority of mercury and chromium are not leached out and are associated with the insoluble fraction of coal, indicating an association with pyrite or silicates.

SUMMARY

Few water-soluble minerals were found in the coals studied. The water-soluble minerals are likely limited to halite (NaCl); gypsum ($CaSO_4 \cdot 2H_2O$), found in the Pittsburgh No. 8 and Illinois No. 6 coals; and sylvite (KCl), found in the Beulah and Illinois No. 6 coals. A small amount of iron was removed from the bituminous coals, most likely from hematite (Fe_2O_3).

High levels of calcium, magnesium, and sodium were removed by ammonium acetate (NH_4OAc). These elements are associated with ion exchange sites of the carboxylic acids in the organic portion of the coal. The lower-grade coals studied contained more organically associated elements.

Iron, calcium, and magnesium are the most commonly removed elements in the acid leaching. The loss of these elements can be attributed to the dissolution of calcite ($CaCO_3$), dolomite ($CaMg[CO_3]_2$), and siderite ($FeCO_3$). The Illinois No. 6 coal had very few elements removed by HCl, indicating few carbonate minerals in the coal and the probable association of mercury and chromium with pyrite and silicates. The calcium present was either in the form of gypsum ($CaSO_4 \cdot 2H_2O$), an accessory element in clays, or organically associated.

In order to predict the behavior of the inorganic portions of the coal during combustion, it is necessary to know how the elements are distributed between the organic and inorganic portions of the coal. The chemical fractionation process helps to define this distribution. The organically associated elements will be freed during the earliest stages of combustion and will react with the inorganic phases as combustion continues. This will have an effect on fouling and slagging within the boiler, reducing plant efficiency. By thorough characterization and careful selection of coals, coal-burning plants can increase efficiency and, in some cases, reduce pollution containing trace elements.

REFERENCES

1. Benson, S.; Holm, P. "Comparison of Inorganic Constituents in Three Low-Rank Coals," *Ind. Eng. Chem. Prod. Res. Dev.* **1985**, *24*, 145-149.

2. Martines-Tarazona, M.; Spears, D.; Tascon, J. "Organic Affinity of Trace Elements in Austrian Bituminous Coals," *Fuels* **1992**, *71*, 909-917.

3. Swaine, D.J. "The Organic Association of Elements in Coals," *Organic Geochemistry* **1992**, *18* (3), 259-261.

4. Miller, R.N.; Given, P.H. *Ash Deposits and Corrosion Due to Impurities in Combustion Gases*, Bryers, R.H., Ed.; Hemisphere Publishing Corp.: Washington, DC, 1977; p 39.

5. Norton, G.A.; Markuszewshi, R.; Buttermore, W.H. "The Removal and Control of Trace Elements in Coal and Coal Wastes," *In* Proceedings of the International Conference on Elemental Analysis of Coal and Its By-Products; 1991, p 270-288.

6. Ciocco, M.V.; Morsi, B.I.; Araujo, G.; Chiang, S.H. "Trace Elements Removal Using a Selective Coal Agglomeration Process," *In* Proceedings of the Ninth Annual International Pittsburgh Coal Conference; 1992, p 299-305.

7. Finkelman, R.B.; Stanton, R.W. "Identification and Significance of Accessory Minerals from a Bituminous Coal," *Fuel* **1977**, *57*, 763-768.

8. Galbreath, K.C.; Brekke, D.W. "Feasibility of Combined Wavelength-Dispersive/Energy-Dispersive Computer-Controlled Scanning Electron Microscopy for Determining Trace Metal Distribution," *In* Draft Proceedings of the Trace Elements Workshop: Trace Element Transformations in Coal-Fired Power Systems; Scottsdale, Arizona, 1993.

9. Wiese, R.G., Jr.; Muir, I.; Fyfe, W.S. "Trace Element Siting in Iron Sulfides from Coal Determined by Secondary Ion Mass Spectrometry," *Energy Source* **1990**, *12*, 251-264.

TABLE 1

Chemical Fractionation Results

Coal — Beulah — Lignite

Elements	Initial, ppm	% Removed by H_2O	% Removed by NH_4OAc	% Removed by HCl	% Remaining
Aluminum	8,100	0	0	33	67
Iron	8,400	0	0	20	80
Titanium	270	0	0	9	91
Calcium	18,000	0	74	24	2
Magnesium	4,600	0	87	6	7
Sodium	5,800	13	87	0	0
Potassium	230	7	43	3	47

Coal — Black Thunder — Subbituminous

Elements	Initial, ppm	% Removed by H_2O	% Removed by NH_4OAc	% Removed by HCl	% Remaining
Aluminum	8,400	0	26	42	32
Iron	1,800	0	0	75	25
Titanium	400	0	0	0	100
Calcium	9,900	0	72	28	0
Magnesium	3,000	0	64	35	1
Sodium	290	27	62	8	3
Potassium	140	0	48	0	52

Coal — Rochelle — Subbituminous

Elements	Initial, ppm	% Removed by H_2O	% Removed by NH_4OAc	% Removed by HCl	% Remaining
Aluminum	8,300	0	0	18	82
Iron	4,600	0	0	96	4
Titanium	2,000	0	0	0	100
Calcium	8,800	0	64	35	1
Magnesium	2,900	0	57	37	6
Sodium	450	11	76	5	8
Potassium	230	0	0	0	100

Coal — Illinois No. 6 — Bituminous

Elements	Initial, ppm	% Removed by H_2O	% Removed by NH_4OAc	% Removed by HCl	% Remaining
Aluminum	15,900	0	0	0	100
Iron	21,100	9	0	0	91
Titanium	610	0	0	2	98
Calcium	5,900	19	74	0	7
Magnesium	750	3	6	0	91
Sodium	1,400	47	17	3	33
Potassium	1,800	2	2	2	94

Coal — Pittsburgh No. 8 — Bituminous

Elements	Initial, ppm	% Removed by H_2O	% Removed by NH_4OAc	% Removed by HCl	% Remaining
Aluminum	12,300	0	0	0	100
Iron	5,200	4	0	39	57
Titanium	580	0	0	0	100
Calcium	330	15	63	10	12
Magnesium	3,300	0	13	15	72
Sodium	420	11	23	0	66
Potassium	1,200	0	0	0	100

TABLE 2

Illinois No. 6 Filtrate Analysis by AA

Elements	% Removed by H_2O	% Removed by NH_4OAc	% Removed by HCl	% Remaining
Arsenic	<7	7	68	18
Chromium	1	1	26	72
Mercury	<24	5	<3	68

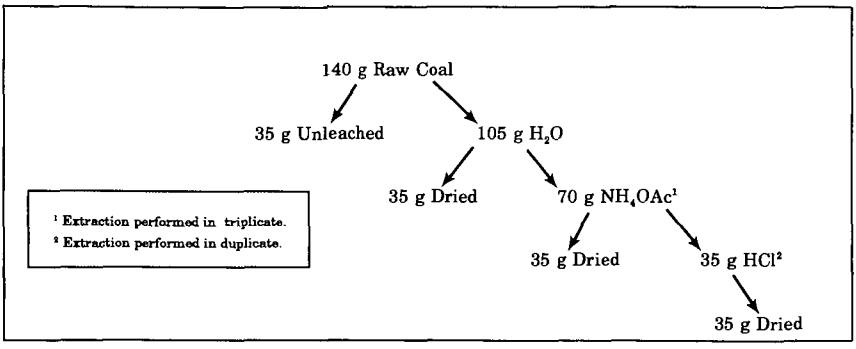

Figure 1. Chemical fractionation procedure.

UTILIZATION OF SPENT OIL SHALE IN A FLUIDIZED BED PROCESS

Asmund Vego, Scott D. Carter and John L. Stehn
Center for Applied Energy Research, University of Kentucky
Lexington, Kentucky 40511-8433

Keywords: Oil shale, Pyrolysis, Gasification, Desulfurization and Combustion

Abstract

The Center for Applied Energy Research (CAER) is currently developing the KENTORT II oil shale retorting process for eastern U.S. oil shales. This is a fully integrated multi-stage fluidized-bed retorting process, which is designed to maximize extraction and utilization of the organic and inorganic components of the shale. After pyrolysis, the spent shale undergoes gasification for generation of hydrogen sulfide and synthesis gas. Combustion of the previously pyrolyzed and gasified shale generates the heat necessary to drive the process.

Introduction

Testing of the KENTORT II retorting concept was initiated in 1986 in a 3.8-cm diameter fluidized bed reactor,[1] and further evaluation was performed in a fully integrated 7.6-cm diameter unit.[2,3] The KENTORT II process is currently being scaled up to a 15.2-cm diameter 23-kg/hr process demonstration unit (PDU). Recent cold flow studies in a full scale model and information from the successful 7.2-cm diameter system provided design data for the PDU.[4,5]

A detailed discussion of the rationale behind the KENTORT II design has been published previously.[6] The primary motivation behind the design was the complete utilization of the spent shale from the pyrolysis step. This is currently not the case for two of the world's largest processors of oil shale, however. The Petrosix process in Brazil currently discards pyrolyzed shale, and this accounts for nearly 50% of the energy losses from the system.[7] The Estonian oil shale industry also discards pyrolyzed shale, and because of the nature of the shale and the process, this results in environmental problems at the shale disposal site.[8] So it is important for process efficiency and sound environmental practices that the pyrolyzed shale be sufficiently utilized within the retorting process. In addition to in-process utilization of spent shale, it may be possible for spent shale to be employed as feedstock for the production of construction materials. Raw Michigan Antrim oil shale is currently in use for the production of portland cement, but it has been suggested that spent shale would be suitable also.[9]

While fluidized bed pyrolysis of oil shale is an efficient method of quickly generating relatively large yields of crude shale oil, substantial amounts of residual carbon and sulfur remain in the spent shale. Traditionally, direct combustion of the char from pyrolysis has been reserved as the method for utilizing the residual carbon. This technique presents two problems when applied to Eastern shales. First, char from fluidized bed pyrolysis contains more carbon than required to provide heat for the retort. It would be necessary to remove substantial amounts of energy from the reactor in order to deplete all the carbon in this manner. Second, the sulfur to carbon weight ratio of pyrolyzed shale is large, which if combusted could produce prohibitive amounts of SO_2.

Steam gasification of the excess carbon from the char represents an alternative to direct combustion. Tests at the CAER have shown that fluidized bed pyrolysis char gasifies readily at 800

°C and 1 atmosphere steam partial pressure.[1] Under these conditions over 40% of the carbon in the pyrolyzed shale was gasified following 30 minutes mean char residence time. Steam fluidization enables also steam/ FeS_x reactions to go nearly to completion. Studies have shown that 90% sulfur removal can be achieved at residence times greater than 30 minutes and temperatures less than 600 °C.[10] Therefore, introduction of an intermediate gasification step between pyrolysis and combustion provides means for attaining total carbon utilization as well as removing substantial amounts of sulfur prior to combustion.

Process Description

The heart of the KENTORT II process (Figure 1) consists of four fluidized bed vessels. The four zones are configured in cascade, where the shale undergoes pyrolysis, gasification/desulfurization, combustion and cooling. The pyrolysis, gasification and cooling sections are aligned vertically and share a common fluidizing gas. Combustion takes place in the fourth bed which is placed adjacent to the other three, and the fluidizing gas is supplied separately. The main body of the KENTORT II unit is constructed from 316 stainless steel. Because of the combination of extreme temperature and corrosive environment in the gasification and combustion section, these sections have been aluminized to prevent scaling and spalling of the reactor material.[5] Aluminizing is a process where aluminum diffuses at high temperature onto the surface of a base metal for a minimum dept of 100 microns, producing an aluminum-rich alloy on the surface. The different sections of the unit are separated by gas distributors which are sandwiched between flanges. The total height of the unit is about 6 meters.

Shale Handling Systems

A screwfeeder is used to meter the shale into the pyrolysis section at a rate of 23 kg/hr. The screwfeeder is supplied by a 140-kg capacity sealed feed hopper. Additional shale can be loaded into the hopper during operation, so truly continuous operation can be achieved. Processed shale at about 400 °C leaves the unit trough an overflow port in the cooling zone. The spent shale is collected in a sealed bin, which may be emptied out during a run to permit lengthy periods of operation. Fines recovered from the pyrolysis cyclone are feed to the combustor by an air lift.

Shale Conveying System

J-valves with corresponding liftpipes provide a conveying system for shale recirculation from the gasification section to the pyrolysis and combustion sections. Solids are transported in a lean phase through the liftpipes, using nitrogen as the carrier gas in the pyrolyzer liftpipe and air as carrier gas in the combustor liftpipe. Nitrogen is used to meter the flow of solids through the J-valves and into the liftpipes. Recirculation rates of up to 90-kg/hr to the pyrolysis section and 225-kg/hr to the combustion section can be achieved simultaneously.

Start-Up System

A propane burner (Figure 2) is used to heat the fluidizing air for the combustor during start-up. By circulating solids among the zones, most of the heat required for preheating is provided by the burner. A superheater upstream of the cooling zone provides the rest of the energy needed to preheat the system. Air, rather than steam, is used during most of the preheating period so that the amount of steam condensate is kept as small as possible. Once steady state conditions are approached, the energy provided by the burner and superheater is reduced or eliminated completely.

Pyrolysis Section

Raw shale is fed over-bed to the pyrolysis section, and a mixture of steam and product gases from the gasification stage below serves as the fluidizing medium. Heat is provided to the pyrolysis section by a combination of fluidizing gas and recirculating solids from the hotter gasification section. The pyrolysis zone has a vertical baffle which splits the section into two equally sized beds. The purpose of the baffle is to narrow the particle residence time distribution by creating two beds in series. By narrowing the particle residence time distribution, greater chemical conversion can occur per unit reactor volume. The operational conditions for the pyrolyzer are: temperature, 500-550 °C; mean shale residence time, 3 minutes; bed depth, 30.5 cm.

Gasification Section

Shale from the pyrolysis section is transferred to the gasification/desulfurization zone by a gravity feed downcomer. The bed depth is designed to be adjustable between 38-76 cm so that solid residence time may be adjusted from 30-60 minutes. Like the pyrolyzer, the gasifier is baffled to narrow the particle residence time distribution. The gasification section is heated by hot solids from the combustion section entering the lower part of the bed, and the operational temperature is from 750 to 850 °C. Steam from the cooling zone below is used as the fluidizing medium.

Cooling Section

A downcomer transfers shale from the gasifier to the cooling section which also serves to preheat the steam that fluidizes the gasification bed. The cooling zone is the primary exit point for solids from the reactor. An overflow outlet in the wall of the vessel creates a 38-cm deep bed.

Combustion Section

The combustor provides the heat required for the pyrolysis and gasification sections of the KENTORT II retort. The gasification and the combustion zones are closely aligned to facilitate the transfer of solids. To minimize mixing of the gas streams, however, the pressure between the two vessels is balanced. The bed depth is 30.5 cm, although this is adjustable by regulating the height of the standpipe. Carbon-containing shale recycled from the gasification section via a pneumatic lift pipe, is the primarily fuel for the combustor. Fines recovered from the pyrolysis cyclone are also fed into the combustor to provide additional fuel. Air is used for fluidization in the combustor.

Oil Collection System

Gases and vapors from the pyrolyzer enter a cyclone for fines removal. A combination convection/liquid-injection heat exchanger then cools the vapor stream to 150 °C which causes an oil aerosol to develop. This aerosol is trapped by an electrostatic precipitator (ESP) which contains approximately 10 m^2 of collection surface area and includes two, two-stage Penney-type collection cells in series to ensure high collection efficiency. Downstream of the ESP, a shell-and-tube condenser is then used to condense steam and light oil that remain. Light oil and water from the condenser are separated, and the water is sufficiently treated to be fed back into the steam generator. Mist collection, further cooling and more mist collection are performed before the gas stream is sampled by an on-line gas chromatograph and mass spectrometer.

Combustion Flue Gas System

Fines are removed from the combustion gas stream by a cyclone before the gas is cooled to approximately 250 °C and released to the ventilation system.

Fines and water are removed from a small portion of the gas stream for analysis by on-line combustion gas analyzers which provide a continuous measure of all major flue gas components.

Discussion

The KENTORT II process utilizes pyrolyzed shale to generate valuable by-products such as elemental sulfur and synthesis gas. The shale is also used to facilitate the operation of the retort by providing the energy to drive the process and the means to transfer this energy throughout the process by recirculating the shale itself. The pyrolysis step of the process actually represents a small fraction of the whole system. It is the additional processing of the shale to extract process heat and by-products that occupies much of the unit. Since fluidized bed pyrolysis is so efficient, the combustion and gasification zones do not make the process any larger than current commercial units which only pyrolyze the shale.[7,8] There is, of course, a point of diminishing returns relating to the carbon utilization of the shale. An objective of the testing with the 23-kg/hr PDU is to evaluate carbon burn-off as a function of gasification and combustion conditions. Once this is complete, an economically-based determination of the optimal carbon burn-off can be made.

It is important from an environmental point of view that the pyrolyzed oil shale be sufficiently processed so that its acid leaching potential upon disposal is not high. The iron disulfide (pyrite and marcasite) content of eastern U.S. shale is high which can lead to acid drainage if these minerals are not converted to FeS (pyrrhotite).[11] Fluidized bed pyrolysis only results in partial conversion of the disulfide to the monosulfide so either combustion or gasification or both, as in the case of the KENTORT II process, is needed so that the conversion is enhanced by the oxidization of the iron. The advantage of using gasification rather than combustion to accomplish this is that H_2S is produced which can be readily scrubbed and converted to elemental sulfur, whereas SO_2 control technology is relatively expensive and inefficient.

The use of the processed shale to transfer heat increases process efficiency in two ways. First, the volumetric heat capacity of shale is high compared to gases which means that large volumes of gas are not needed to heat the system. Second, by using the shale, which is present in the system anyway, rather than an added heat-transfer material, the need for a step to separate the shale from the heat carrier is eliminated. The properties of the shale will dictate the extent to which pyrolyzed shale can be used as the heat carrier. The shales of the eastern U.S. are fairly refractory and can be processed at high temperatures with relatively little decrepitation. The Western shales on the other hand lose their strength when subjected to normal combustion or gasification temperatures because of their high carbonate content; therefore, processes which have been designed for Western shale that combust the spent shale utilize combustion temperatures of less than 700°C.[12]

Summary

A 23-kg/hr integrated fluidized bed Process Demonstration Unit (PDU) called the KENTORT II, has been built at the Center for Applied Energy Research. The PDU effectively utilizes the organic and inorganic components of eastern U.S. oil shales through pyrolysis, gasification/desulfurization and combustion. Autothermal operation is achieved by combustion of the residual carbon following pyrolysis and gasification. Heat is transferred among the different sections of the unit by recirculation of hot combusted solids. The main product from the KENTORT II is a high yield of liquid hydocarbons from the pyrolyzer, and important by-products include elemental sulfur (from hydrogen sulfide gas) and synthesis gas.

Acknowledgements
This work was supported in part by the Morgantown Energy Technology Center, USDOE, under Cooperative Agreement DE-FC21-90MC27286 (such support does not constitute an endorsement by the USDOE of the views expressed in this article).

References
1. Rubel, A.M and Davis, E., "Evaluation of the Gasification Potential of Kentucky Oil Shale Char Produced Under High Yield Fluid Bed Conditions," 1987 Eastern Oil Shale Symposium Proceedings, Univ. of Kentucky, Lexington, Ky.

2. Carter, S.D., Robl, T.L., Rubel, A.M., and Taulbee, D.N., "Processing of Eastern U.S. Oil Shale in a Multistaged Fluidized Bed System," Fuel, 1990, 69, 1124.

3. Carter, S.D., Robl, T.L., Taulbee, D.N., and Rubel, A.M., "Testing of an Irati Oil Shale in a Multistaged Fluidized Bed System," Fuel, 1991, 70, 1347.

4. Vego, A., Carter, S.D., Stehn, J.L. and Neathery, J.K., "Scaleup of the KENTORT II Process, Cold Flow Modeling of the 50-lb/hr. retort", 1991 Eastern Oil Shale Symposium Proceedings, University of Kentucky, Lexington, KY.

5. Carter, S.D., Rubel, A.M., Robl, T.L., and Taulbee, D.N., "The development of the KENTORT II Process for Eastern U.S. Oil Shale", Final Report for U.S. Department of Energy, Cooperative Agreement NO: DE-FC21-86LC-11086.

6. Carter, S.D., "The KENTORT II Concept: A Process Description," 1987 Eastern Oil Shale Symposium Proceedings, Univ. of Kentucky, Lexington, Ky.

7. Lisboa, A.C., Novicki, R.E., and Piper, E., "Petrobras Boosts Oil Shale Fines Processing," 1989 Eastern Oil Shale Symposiumn Proceedings, University of Kentucky, Lexington, Ky.

8. Urov, K., 6th Australian Workshop on Oil Shale, 1991, Univ. of Queensland, St. Lucia, Brisbane, pp. 25-31.

9. Schultz, C.W., Lamont, W.E., and Daniel, J., "The Use of Devonian Oil Shales in the Production of Portland Cement," 1991 Eastern Oil Shale Symposium Proceedings, Univ. of Kentucky, Lexington, Ky.

10. Carter, S.D. and Taulbee, D.N., "Fluidized Bed Steam Retorting of Kentucky Oil Shale," Fuel Processing Technology, 1985, 11, 285.

11. Robl, T.L., Barron, L.S., Schram, W., and Thomas, G., 1988 Eastern Oil Shale Symposium Proceedings, IMMR88/101, University of Kentucky, Lexington, Ky.

12. Lewis, A.E., Braun, R.L., and Diaz, J.C., 17th Oil Shale Symposium Proceedings, 1984, Colorado School of Mines, pp. 1-16.

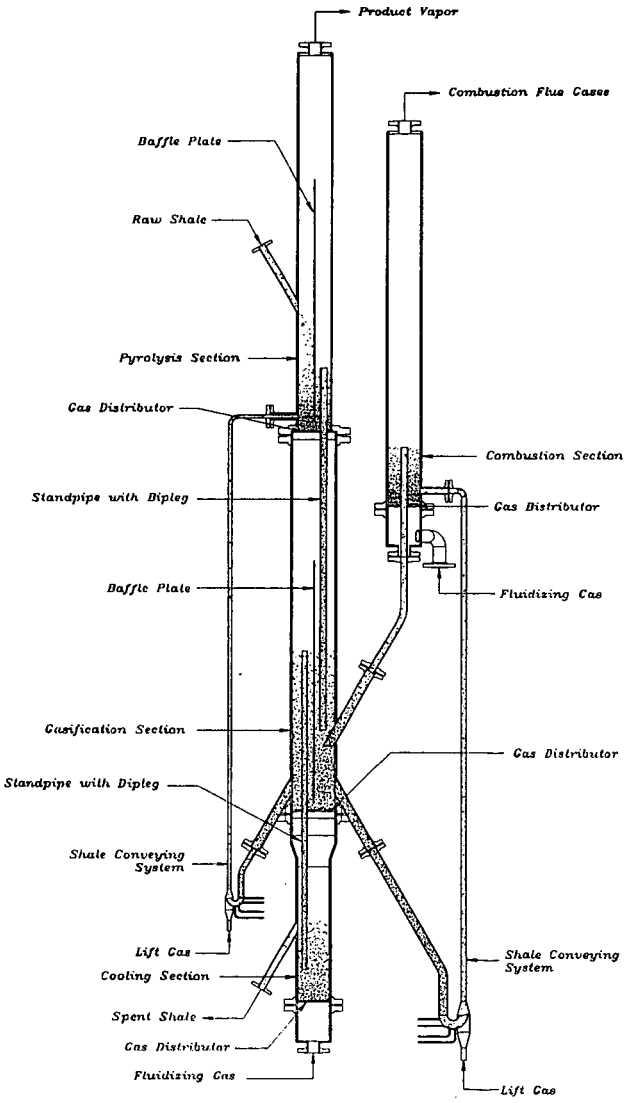

Figure 1. KENTORT II Reactor with Internals

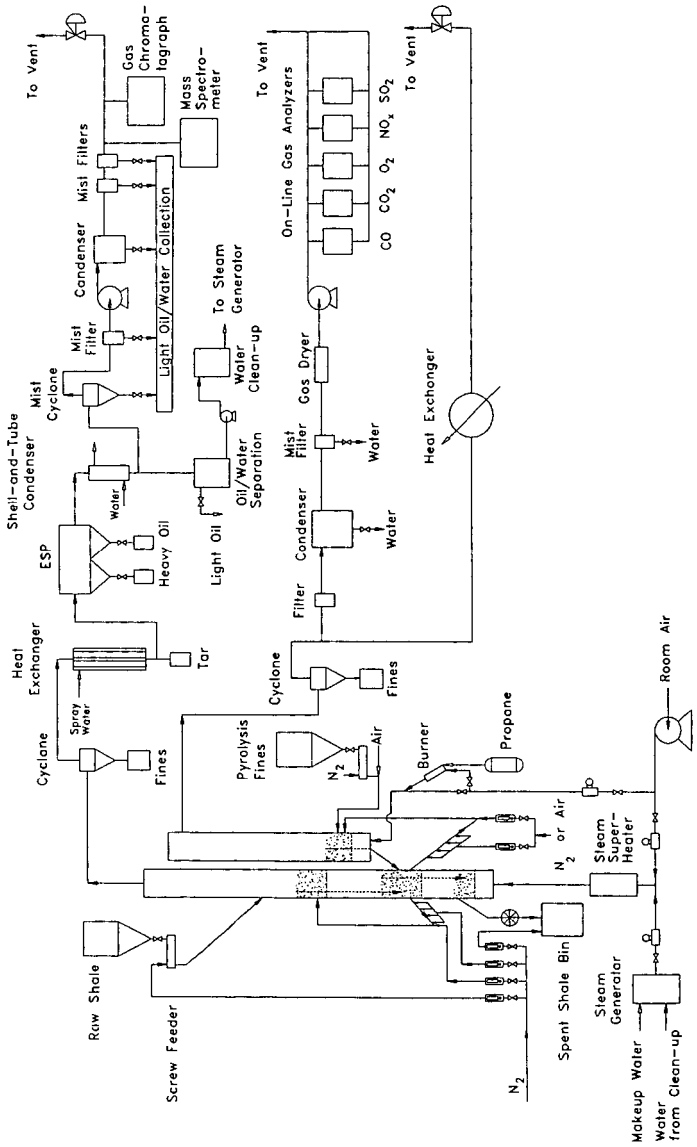

Figure 2. Simplified Flow Diagram of the 23-kg/hr KENTORT II Retort

ROLE OF BIOFUELED GAS TURBINES IN SOIL REMEDIATION

Joseph T. Hamrick
Aerospace Research Corporation
5454 Aerospace Rd.
Roanoke, VA 24014

Keywords: Biomass Fuel, Gas Turbines, Power Generation, Soil Remediation

INTRODUCTION

Clean up of soils polluted with metals pose difficult and expensive problems in many places around the world. Remediation has ranged from vitrification of the polluted soil to disposal in landfills. Dr. Rufus L. Chaney, reference 1, has proposed "Green Remediation" as a means of treatment. "Green Remediation" relies on the ability of plants to accumulate metals from the soil. Upon reaching maturity the plants can be harvested and burned with subsequent recovery of the metals from the ash. Some specifics of growth, species selection, and various aspects of agronomic management are covered in reference 1. It is the purpose of this presentation to introduce the prospect of using a biomass fueled gas turbine power generating system as a remediation vehicle in conjunction with growth of metal accumulating plants some of which have been given the name "Hyperaccumulators". The biofueled gas turbine power generating system is described and various aspects of its use are presented in references 2, 3, & 4.

BACKGROUND INFORMATION

The use of metal accumulating plants as fuel was first brought to the attention of Aerospace Research Corporation by Dr. Barry Noval and Lionel Gillston of Energy Products Enrichment, Inc. of Norristown, Pa. They suggested a multiple use of the biomass fueled gas turbine in which operation with metal accumulating plants would produce an ash-ore product that could be smeltered to recover the metal. In areas where the contaminated land could not support full time operation, nonpolluted land growing crops such as sweet sorghum together with sawmill waste, demolition waste, and clean municiple waste could be used.

Conversations with Dr. Robert P. Bosshart of Horsehead Resource Development Company, Inc. of Palmerton, Pa. revealed that there is considerable interest within that company in use of metal accumulating plants to clean up contaminated soil. Soils in the Palmerton area where zinc smelters are located have become contaminated over the years. One problem is that much of the contaminated land is too steep to cultivate by conventional methods. An estimated 1000 acres of level land may be available for use in a remediation program. Sixty to eighty percent of the fuel needed for an economical biomass fueled gas turbine installation would have to come from other sources.

Throughout the U.S. and the world there are large land areas that have become contaminated with metals such as lead, copper, zinc, cadmium, arsenic, and nickel and may be candidates for phytotreatment. While it may be desirable in some cases to delay installation of phytotreatment systems until more research is performed on candidate metal accumulators, there are many locations where biomass fueled power generation systems may be installed and economically operated with marginal accumulators. Under the Public Utilities Regulatory Policies Act power companies are required to purchase the power at their avoided energy costs. Growth, harvesting, transportation, storage, and processing of the biomass fuel and ash disposal constitute the main differences in the biomass fueled gas turbine power generating systems and those now in operation and use with petroleum and gaseous fuels around the world.

GROWTH OF METAL ACCUMUULATORS

As pointed out in reference 1, the metal accumulators may be specific in their tolerance for the contaminating metals. The selection of species will require agronomic expertise and will involve soil analysis, not only from standpoint of metal contamination but also from standpoint of alkalinity and nutrient content. A mixture of plant species may be required to accommodate multiple contaminants and erosion control. It is pointed out in reference 1 that few hyperaccumulators are available which generate substantial biomass. A low level accumulator which generates substantial biomass may achieve the same metal uptake for a given area as a hyperaccumulator with low biomass production. The higher biomass production would improve the economics of power generation. In climates with short frost free seasons it may be necessary to grow a variety of crops to support a power system. For example, bagasse from sorghum which constitutes substantial biomass for fuel after the sweet juice is extracted is seasonal. However, elemental analysis of sweet sorghum bagasse show the presence of chromium, barium, nickel, zinc, and copper among the lighter metals. Therefore, it is a good accumulator candidate. It can be grown in combination with hyperaccumulators as well as high producing legumes and grasses.

TRANSPORTATION AND STORAGE

Transporting and storage of biomass presents an economic problem because of its low density. For that reason it is important that hauling distances be short and storage operations be well planned. Legumes and grasses can be round baled and stored in the field near roads where they can be picked up and hauled to the point of use. The bales can be capped with plastic or left exposed to the weather. Both practices are followed throughout the United States. The storage of sweet sorghum is more complex. It is estimated that the harvesting and processing of sweet sorghum can be stretched out over a period of approximately six months in single crop climates. Mixing of varieties and staggered plantings will be required. The six month estimate is based upon information contained in references 5 and 6. The bagasse remains of the sorghum have to be dried and put in covered storage to prevent deterioration from fermentation. Providing covered storage for the large amounts of bagasse that would be required for year round use may not be practical. In tropical areas where year round growth of sweet sorghum is possible, the storage problem is minimal.

PROCESSING

Densification of legumes and grasses is necessary for feeding into the pressurized combustion chamber. Densifying involves grinding, pelleting, and crumbling. Efficient machines are commercially available for accomplishment of all three tasks. The pelleting process requires steam which can be supplied by a waste heat boiler heated by the turbine exhaust gases. Use of some of the generated electricity will also be required. Extraction of the juice from sweet sorghum may be accomplished by grinding or squeezing through rolls. The product from either process is referred to as bagasse. Bagasse from grinding can be dried and with little further screening or grinding be fed into the combustor. The bagasse from squeezing retains its identity as a stalk and must be subjected to substantial grinding before drying and feeding into the combustor. The sweet juice can be reduced to syrup with heat from the gas turbine exhaust. Storage of the syrup will allow year round operation of an ethanol plant. The seed head on the sorghum can also be used in ethanol production.

DISPOSAL OF THE ASH

The ash generated in the combustion chamber passes with the hot gases to a cyclone filter. The ash falls to the bottom of the cyclone where it is recovered, and the cleaned hot gases are ducted to the turbine. The cleaned gases normally contain 35 to 50 parts per million of particles that are on the order of 2 micrometers or less in diameter. The heavy metal content of the particles and any hazard potential will have to be evaluated. It is expected that particles containing heavy metal constituents will be more completely filtered due to higher density.

Biomass ash normally contains a commercially recoverable amount of potassium oxide which reacts with water to form highly soluble potassium hydroxide. Leaching of the potassium hydroxide while leaving the generally insoluble heavy metal oxides in the ash is one approach to recovery of the potassium.

The metal content of the ash will depend upon the variety and types of plants being used as a fuel as well as the condition of the soil in which the plant is grown. If the metal can be economically recovered and the residue from the recovery process is free of contaminating metal, the ash may be returned to the soil. If it is uneconomical to recover the metal, the most economical disposition probably will be into a qualified landfill.

ECONOMIC CONSIDERATIONS

The objective in using biofueled gas turbine power generating systems in soil remediation is to reduce clean up costs or to turn a profit if possible. The payment received for the generated power is the key factor. The avoided energy costs for power that public utilities are required to pay in complying with the Public Utilities Regulatory Policies Act will not normally be adequate to allow economical use of fuels other than waste products such as sawdust. Utilities with power plants located near coal mines generally have avoided energy costs less than 2¢/kw hr. with a charge to customers of 5¢ to 8¢/kw hr. Businesses generally pay a demand penalty in addition. Paper mills in coal producing areas are large users of sawdust and bark in their boilers. With 1993 prices for coal it is more economical for paper mills to switch to coal when the price of sawdust approaches $28 per ton on a bone dry basis. To compete with coal would require production of approximately ten tons of dry biomass per acre at $280.00 per acre. To meet a production goal of ten dry tons per acre probably would require harvesting a summer crop of sweet sorghum plus a winter cover crop in the northeastern part of the U.S. where there is an identified need for remediation. Unless there is a very large acreage, for example, five thousand acres of land to be remediated, reliance upon waste products for supplemental fuel probably would be the most economical approach.

In addition to bagasse, the sweet sorghum in the northeastern part of the U.S. would produce approximately 1.5 tons of sugar per acre which is equivalent to approximately 130 gallons of ethanol. The heat from the gas turbine exhaust can be used for processing the ethanol. An industrial user of power that has land to be remediated may well profit from generation of its own power with sale of the excess to a utility.

SUMMARY

Of the methods available to effect soil remediation phytotreatment of contaminated soils promises to be the most economical. The number of years required to accomplish the task will depend upon the skillfulness in soil management, the

variety of plants used, and the severity of the contamination. The ability to turn a profit with burning of the biomass in a gas turbine power generating system will depend upon the payment received for the power produced, payment for by-products, operating costs, cost of biomass production, and availability of waste for alternate fuel. By-products will consist primarily of potassium and the metal of contamination. In the case of sweet sorghum, ethanol produced from the sweet juice would be a major by-product. Biomass waste from sawmills and demolition can fill in during seasonal lulls in crop production.

REFERENCES

1. Cheney, Rufus L. "Revival Field", A Test of "Green Remediation", Soil Microbial Systems Laboratory USDA - Agricultural Research Service, Beltsville, MD 20705.

2. Hamrick, Joseph T., Biomass Fueled Gas Turbine Development, ACS Symposium Series 515 Clean Energy from Waste and Coal, M. Rashid Khan, Editor Aug. 25 - 30, 1991 American Chemical Society, Washington, D.C.

3. Hamrick, Joseph T., Worldwide Role of Gas Turbine Power Generation with Biomass Fuels, Volume 4 No. 4 World Resource Review, International Journal Dec. 1992, 7501 Lemont Suite 335, Woodridge, IL 60517-2661.

4. Hamrick, Joseph T., The Biomass Fueled Gas Turbine; One Answer to Global Warming, Global Gas Turbine News, May 1992, International Gas Turbine Institute, American Society of Mechanical Engineers, 6085 Barfield Road Suite 207, Atlanta, GA 30328.

5. Parrish, David J. and Cundiff, John S., Long-term Retention of Fermentables During Aerobic Storage of Bulked Sweet Sorghum, Departments of Agronomy & Agricultural Engineering, Virginia Tech April 1985.

6. Gascho, Gary J., The Potential Length of the Harvest Period For Sweet Sorghum, Agronomy Department, Coastal Plain Experiment Station, University of Georgia, Tifton, GA, April 1983.

From a literature search in 1992 by Dr. Shu-I Tu and associates of the Plant and Soil Biophysics Research Unit of the North Atlantic Area Regional Research Center of the U.S. Department of Agriculture the following individuals have been working on the selection of plant varieties with unique abilities to accumulate certain metals: R.B. Clark of University of Nebraska, E.A. Brams of Prairie View A&M University in Texas (university information number is 409-857-3812), D.R. Parker of the University of California at Riverside (department phone number is 907-787-5116), Dr. Grunes and collaborative with ARS at Ithaca, NY (607-255-3003), and V.V. Baligar with ARS at Beckley, WV (center information number is (304-252-6426). G.N. Richard at the University of Montana at Missoula (campus information number is 406-243-0211) has been working on the influence of cations pyrolysis of wood. The assistance of Dr. Shu-I Tu is appreciated.

MATHEMATICAL ANALYSIS OF A MSW ROTARY INCINERATOR

James T. Cobb, Jr. and K. Banerjee

Department of Chemical & Petroleum Engineering
University of Pittsburgh
Pittsburgh, Pennsylvania 15261

Keywords: municipal solid waste, incineration, mathematical model

ABSTRACT

A computerized mathematical model of a refractory-lined rotary kiln combustor with a vertically well-mixed bed has been developed. Bed height varies with horizontal distance as fuel is consumed. The kiln contains a pyrolysis zone, followed by a combustion zone. A kinetic model for cellulose pyrolysis simulates the thermal destruction of MSW in the first zone. The combustion of particles in the second zone follows a shrinking-core model. Model behavior is in good agreement with the performance of commercial units.

INTRODUCTION

A number of the waste-to-energy facilities operating in the United States utilize a rotary kiln combustor as the principal treatment unit in their systems. The barrel of the kiln may be either refractory-lined or water-walled. Waste is fed to the kiln from a receiving system and the products of combustion are treated and released. The combustion gases are polished in a secondary combustor, cleaned of acidic components and particulates, and sent to a stack. Bottom ash is cooled, mixed with fly ash, stabilized and landfilled.

Because of the concerns for full burnout of the combustibles in the feed, the destruction of toxic organics, the segregation and collection of toxic metals, and the efficient collection of energy, developers and operators of MSW kiln combustors must have a thorough understanding of the operation of each element of their waste-to-energy facilities and of the integration of these elements. The mathematical model described in this paper has been constructed and tested to assist in better understanding the operation of the rotary kiln combustor at the heart of many such facilities.

KINETIC MODEL

Incineration is a complex physical and chemical process [1]. Waste fed to the rotary kiln first is demoisturized and heated. When it reaches its reaction onset temperature, pyrolysis, sublimation and other solid volatilization reactions occur under starved-air conditions. After these are complete, the char remaining is oxidized under excess-air conditions. For manageability of the final kiln combustor model developed in this study, a simple kinetic model for cellulose pyrolysis has been adopted to describe the pyrolysis of waste in the starved-air region of the kiln [2]. In addition, the assumption has been made that the surface oxidation of char in the

excess-air portion of the kiln is rapid and is largely controlled by the mass transfer of oxygen through the bed.

The kinetic model for the pyrolysis of cellulose is based upon experimental work in the temperature range of 300°C to 1000°C. In its simplest version, the model assumes that cellulose decomposes directly to each reaction product, *i*, by a single, independent reaction pathway,

$$\text{cellulose} \xrightarrow{k_i} \text{product } i$$

and that the kinetics of this process can be modeled by a unimolecular first-order reaction having a rate constant that may be written in the Arrhenius form,

$$\frac{dV_i}{dt} = k_i \, exp\left(\frac{-E_i}{RT}\right)\left[V_i^* - V_i\right]$$

where V_i is the percent yield of gas *i* at any time t, V_i^* is the ultimate (maximum) yield of gas *i*, and k_i and E_i are kinetic parameters. These parameters were correlated with gas-phase pyrolysis products, observed by experimentation, including light hydrocarbons, alcohols, aldehydes, acids, H_2, H_2O, CO, CO_2 and tar.

Two modifications of the kinetic model were required before it could be applied to MSW incineration. First, the rate expressions had to be rewritten so as to account for the decomposition of tar to smaller gaseous species. In order to achieve this, it was assumed that the tar decomposed in the same proportion as the ultimate yields of the various species. A modified ultimate yield was therefore defined according to,

$$V^*_{m,i} = V_i^* + \frac{V_i^*}{\sum_{i=1}^{n} V_i^*} V^*_{tar}$$

were n is the number of gaseous species evolved during pyrolysis. Secondly, the discrete rate equations were combined, using the modified ultimate yields, to achieve a mass balance.

To reach the char surface and combust the carbon there, the oxygen is assumed to diffuse through the bed to the individual char particles and then through the inert ash layer to the surface of the carbon. The carbon core shrinks as the combustion reaction proceeds. However, the total particle radius remains constant due to the formation of the ash layer, with an accompanying increase in particle porosity. Although the model can account for a particle size distribution of char, for the purpose of this study a uniform particle size has been considered. A mass balance is performed on selected individual particles throughout the bed, using a shrinking core modeling technique [3] to calculate the burning rate of the particles.

KILN COMBUSTOR MODEL

Previous mathematical models for rotary combustors have been developed and described by Essenhigh and Kuo [4], Gorog [5], Ghoshdastidar et al. [6], Jang and Acharya [7], Silcox et al. [8], Ghezzi et al. [9], Wormeck and Pershing [10], Lemieux et al. [11] and Sethi and Biswas [12].

In this study the kiln is divided into two active zones - a first zone for pyrolysis and a second zone for combustion. The model for the pyrolysis zone relies upon the following assumptions:

- bed height decreases linearly with distance along the kiln's centerline;
- the bed is well mixed in the vertical direction;
- only convective heat transfer from the gas to the bed is considered; the kiln wall is assumed to be refractory-lined, thus no heat is transferred through the barrel;
- the temperature in the product gas above the bed is constant throughout this zone of the kiln; its value is calculated by the method of Tillman [1];
- both the solid and gas regions operate in the plug-flow regime.

The model for the combustion zone is based upon the model for zirconium combustion, developed by Lemieux et al. [11] The bed depth and the uniform temperature throughout the bed are set at the values obtained at the exit of the pyrolysis zone. The model determines the burning rate of the char and calculates the char mass flow profile across the combustion zone. The bed is axially divided into slices of uniform surface oxygen concentration and each axial slice is divided vertically into segments of uniform oxygen concentration and particle size. A mass balance is performed on the slices in the vertical direction, yielding an ordinary differential equation describing diffusion of oxygen through a porous solid, with boundary conditions at the wall-solid and gas-solid interface. The particle burning rate (calculated as defined earlier) is combined with equations used to describe oxygen transport through the bed. Oxygen is assumed to be at a uniform concentration at each bed depth location, and the particles are assumed to be small enough that oxygen is at a uniform concentration in the gas surrounding each particle. The resulting finite difference equations are solved using a tridiagonal matrix algorithm.

The residence time of char in the kiln was calculated according to [13],

$$\theta = \frac{0.19L}{NDS}$$

where Θ is expressed in minutes, L is the kiln length, D, the kiln diameter, N, the number of revolutions of the kiln per minute and S is its inclination to the horizontal.

The complex three-dimensional nature of the kiln, with variations in the x, z and ϕ directions necessitates simplifications to enable a solution of the model equations. The bed height, t_b, is that corresponding to the one required for a bed with the same cross-sectional area and the same area exposed to the gas as in the

actual kiln. It is reasonable to assume that the bed height remains constant in the burnout zone because char constitutes but a small fraction of the solids in this zone.

RESULTS FROM USING THE MODEL

Physical parameters required by the model were derived from the MSW incineration facility located at McKay Bay, a suburb of Tampa, Florida [14]. The sources of values of the various fundamental parameters required by the model are detailed in Reference 15. This reference also includes a discussion of the method used to solve the set of ordinary differential equations that constitute the pyrolysis model and the tridiagonal matrix, which is derived from the linear finite difference equations that constitute the combustion model. The FORTRAN code is also provided.

The cellulose and char mass flow profiles for a base case where the McKay Bay facility is operating at 77% of its design capacity are shown in Figures 1 and 2. Three distinct regions exist in Figure 1, which shows the results of the pyrolysis model. A significant portion of the kiln length is taken up by the heatup zone in which the MSW is raised to the reaction onset temperature. This is achieved by auxiliary fuel usage. Farther down the kiln is a short reaction zone in which pyrolysis of the waste occurs. This zone is characterized by a fall in the cellulose mass flowrate and a concomitant increase in that of the char. The third zone, where the pyrolysis model shows a constant char flowrate, and is in reality the burnout zone, is more appropriately described in Figure 2 by the results of the combustion model. Note that the abscissa has been shifted between Figures 1 and 2, such that the origin for Figure 2 is placed at the beginning of the burnout zone.

Bed temperature profiles through the heatup and reaction zones are shown in Figure 3 for the base case (9,400 kg waste/hr) and a case of further reduction in flow (4,500 kg waste/hr). This is an example of the use of the model to conduct parametric studies. Figure 3 indicates that the bed temperature is fairly insensitive to changes in the MSW feedrate. This could perhaps be justified by recalling that the bed is fairly well mixed and also that at a constant fuel-air ratio the flame temperature remains constant due to a balance between the reactive heat input and the convective heat removal. In operating incinerators the bed temperatures have been observed to be markedly different for different solids feedrates. This could result if the fuel-air ratio is not held constant during such experiments. Then again, incorporation of the radiative component of heat transfer could result in temperature profiles which match the actual trends better.

Another example of a parametric study is shown in Figure 4, which examines the relatively significant effect of bed porosity (0.54 void fraction - the base case - vs. 0.675 void fraction) on the rate of combustion in the burnout zone. Higher values of porosity reduce the length of this zone because the oxygen has better access to the char.

CONCLUSIONS

The mathematical model of a rotary kiln MSW combustor successfully predicts important aspects of its overall performance and several trends involving parametric variations in its operation. The size of the heatup zone, the size of the reaction zone, and the carbon burnout are quite accurate. However, temperature responses to changes in the MSW feedrate and the size of the burnout zone do not conform strictly to operational experience.

The current model, as well as improved future versions, should prove helpful in the analysis and design of waste-to-energy facilities employing this technology. The analysis of bed porosity has already shown that this parameter is a key factor in the performance of the burnout zone. Analysis of the heatup zone suggests that, because this region appears to require a major portion of the incinerator, preheat of the MSW feed by exiting flue gases might increase kiln capacity.

REFERENCES

[1] Tillman, D. A., et al., Incineration of Municipal and Solid Hazardous Wastes, Academic Press, 1989, p. 21.

[2] Hajalogol, M. R., et al., Ind. Eng. Chem. Process Des. Dev., 21, 457, 1982.

[3] Levenspiel, O., Chemical Reaction Engineering, John Wiley & Sons, 1977, p. 466.

[4] Essenhigh, R. H., and T. J. Kuo, Second Incineration Conference, Chicago, IL, 1965.

[5] Gorog, J. P., et al., Metall. Trans., **13B**, 153, 1982.

[6] Ghoshdastidar, P. S., et al., ASME National Heat Transfer Conference, Denver, CO, 1985.

[7] Jang, D. S., and S. Acharya, AIChE Annual Meeting, New Orleans, LA, 1988.

[8] Silcox, G. D., and D. W. Pershing, AIChE Annual Meeting, New Orleans, LA, 1988.

[9] Ghezzi, U., et al., Proceedings of the Intersociety Energy Conversion Engineering Conference, Piscataway, NJ, 1988.

[10] Wormeck, J. J., and D. W. Pershing, Proceedings of the ASME National Heat Transfer Conference, Houston TX, 1988.

[11] Lemieux, P. M., et al., Waste Management, **9**, 125, 1989.

[12] Sethi, V., and P. Biswas, JAPCA, **40**, 42, 1990.

[13] Theodore, L., and Reynolds, Introduction to Hazardous Waste Incineration, John Wiley & Sons, 1987, p. 248.

[14] Waste Management, Inc., Fact Sheet and Project Description of the McKay Bay Refuse-to-Energy Facility, Tampa FL, 1985.

[15] Banerjee, K., MS Thesis, University of Pittsburgh, 1990.

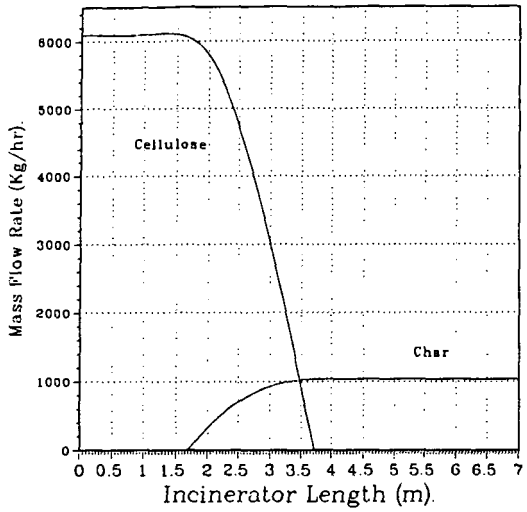

Figure 1. Mass Flow Profiles for the Base Case

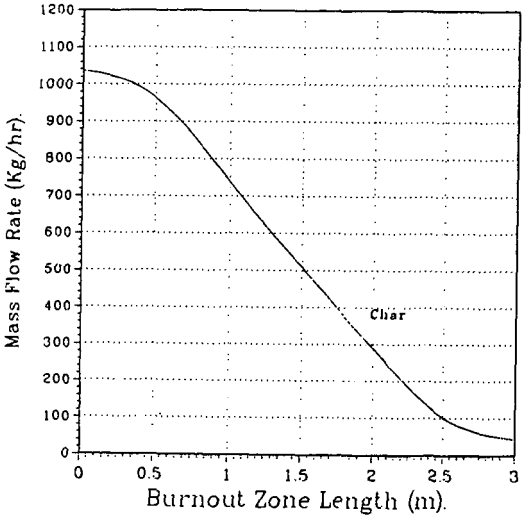

Figure 2. Char Mass Flow Profile in the Burnout Zone

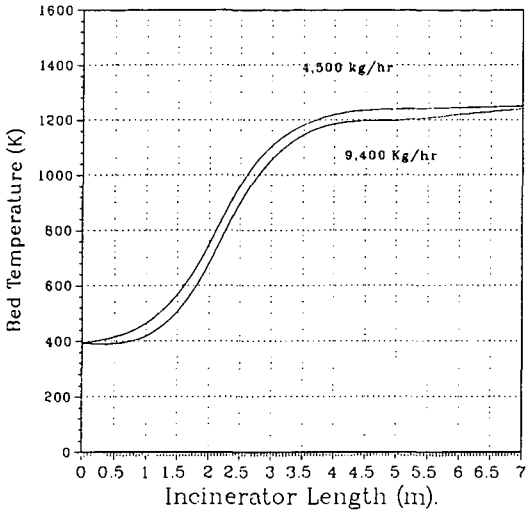

Figure 3. Bed Temperature Profiles

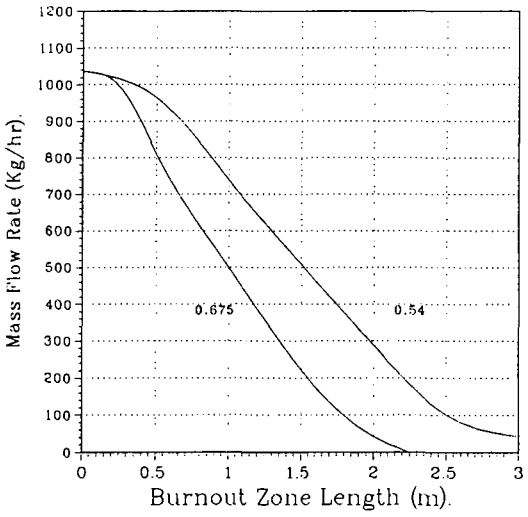

Figure 4. Effect of Bed Porosity

ENERGY AND MASS BALANCE CALCULATIONS FOR INCINERATORS

C.C. Lee and G.L. Huffman
U.S. Environmental Protection Agency
Risk Reduction Engineering Laboratory
Cincinnati, Ohio 45268

ABSTRACT

An estimate of an energy and mass balance within an incinerator is a very important part of designing and/or evaluating the incineration process. This paper describes a simple computer model which is used to calculate an energy and mass balance for a rotary kiln incinerator. The main purpose of the model is to assist EPA permit writers in evaluating the adequacy of the data submitted by incinerator permit applicants. The calculation is based on the assumption that a thermodynamic equilibrium condition exists within the combustion chamber. Key parameters which the model can calculate include:

- Theoretical combustion air;
- Excess air needs for actual combustion cases;
- Flue gas flow rate; and
- Exit temperature.

INTRODUCTION

Although there are many potential hazardous waste treatment technologies, current data indicate that no other treatment technology is as universally applicable as incineration to treat the many different types of hazardous waste. A recent survey showed that more than 80% of the technologies used to remediate Superfund sites are incineration-related technologies (Lee, 6/90). As a matter of fact, incineration has been considered to be a proven technology in many of the regulations developed under the various environmental laws enacted to cover the treatment/disposal of the different types of solid wastes; for example:

(1) Hazardous, medical and municipal waste as regulated under the Resource Conservation and Recovery Act (RCRA);

(2) Industrial and municipal sludge waste as regulated under the Clean Water Act;

(3) Pesticide waste as regulated under the Federal Insecticide, Fungicide and Rodenticide Act (FIFRA);

(4) Superfund waste as regulated by the Superfund Amendments and Reauthorization Act (SARA); and

(5) Toxic substances as regulated under the Toxic Substances Control Act (TSCA).

In addition, incineration facilities are subject to the regulations under the Clean Air Act and numerous State and local requirements.

One of the key factors necessary to ensure the safe incineration of various wastes is for a permit writer to fully understand the incineration process and to adequately check or specify permit conditions at an incineration facility that has come under his or her scrutiny. However, this not an easy task for the following reasons:

- In many cases, the incineration facility is site-specific and process-specific. In other words, different incinerators use different destruction processes and different pollution controls.
- In reviewing a permit application, a permit writer often is confronted with the complex and highly uncertain task of determining whether data submitted are adequate or accurate. For example, if an applicant's data show that his incinerator can reach a certain temperature by burning certain wastes at certain combustion air levels, the question is, "Are the claimed data dependable?"
- In issuing a permit, a permit writer needs to make decisions regarding how to approve or how to specify permit conditions which, for obvious reasons, involve costs and the personnel needed for that industry to comply with the final permit.

The Risk Reduction Engineering Laboratory (RREL) of EPA's Office of Research and Development in Cincinnati has been supporting EPA's RCRA permit writers regarding how to appropriately evaluate a permit application. One of the products from this support effort has been the development of the Energy and Mass Balance Model for Incinerators. The model was intended to assist a permit writer in quickly evaluating whether or not an incineration applicant's claimed data are based on sound engineering principles and are dependable. However, the model involved many complex submodels and are compiled in a computer diskette. Presently, a user cannot see the detailed steps which are built into the software in order to edit the calculation procedures to serve his own specific calculational needs. To overcome this model disadvantage, the authors used the model concept and wrote a program on Lotus 1,2,3 to compare the calculated results with an actual case for which measurement data were available. The results will show that the calculated data are reasonably consistent with the actual trial burn data.

STATEMENT OF THE PROBLEM

A Ciba-Geigy rotary kiln incinerator was chosen as the basis for the calculation. The schematic of the Ciba-Geigy incinerator is shown in Figure 1 (EPA 9/86).

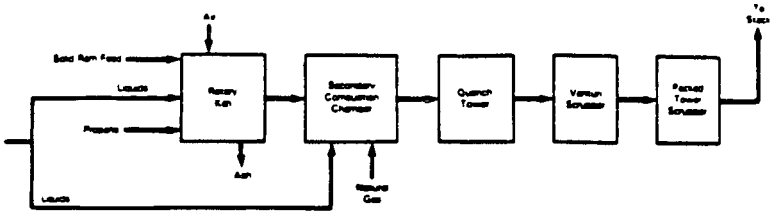

Figure 1. Process Flow Diagram of Ciba-Geigy Incinerator

Ciba-Geigy sponsored a trial burn on November 12-17, 1984. The measured data was later summarized in an EPA report (EPA 9/86) and key aspects of it appear below.

Equipment Information:

- Type of unit: Private incinerator-Rotary kiln with secondary chamber, Vulcan Iron.
- Capacity: 50 tpd (tons per day) with 10% excess capacity (30 x 10^6 Btu/h for each burner)
- Pollution control system: Quench tower, Polygon venturi scrubber (25-in. pressure drop), and packed tower scrubber.
- Waste feed system:
  - Liquid: Hauck Model 780 wide range burners (kiln and secondary burners)
  - Solid: Ram feed
- Residence time: 5.05 s (kiln); 3.09 s (secondary chamber)

Test Conditions:

- Waste feed data: Hazardous liquid and nonhazardous solid wastes usually burned; for this run, only, synthetic hazardous liquid waste was tested
- Length of burn: 6 to 9 h (2-h sampling time)
- Total amount of waste burned: 480 gal (liquid) and 0 lb (solid)
- Waste feed rate: 4 gpm (liquid); 0 lb/h (solid)

- POHCs (Principal Organic Hazardous Constituents) selected and concentration in waste feed:

Name	Concentration, %
Hexachloroethane	4.87
Tetrachloroethene	5.03
Chlorobenzene	29.52
Toluene	60.58

- Btu content: 15,200 Btu/lb
- Ash content: Not measured
- Chlorine content: 20.8% (calculated)
- Moisture content: Not measured

Operating Conditions:

- Temperature: Range 1750° - 1850°F (kiln); 1950° - 2050°F (Secondary chamber)
- Average 1800°F (kiln); 2000°F (Secondary chamber)
- Auxiliary fuel used: Natural gas
  - Primary kiln 1200 scfh natural gas; Secondary chamber 900-1300 scfh
- Airflow:
  - Primary air to kiln: 2200 cfm
  - Secondary air to kiln: 1400 cfm
- Flue gas oxygen content: 10.3%

ENERGY AND MASS BALANCE CALCULATIONS [For Primary Chamber (Kiln) Only]

a. Given Conditions

a1.	Waste feed rate (gpm):	4 gpm	
	Assume that 1 gal =	5 lb	
	Waste feed rate in lb/hr:		1200 lb/h
a2.	Fly ash (% of waste feed):		0 (assumed)
a3.	% of ash due to unburned carbon:		0 (assumed)
a4.	Ash quench temperature:	undefined	
a5.	Exit temperature:	unspecified	
a6.	Reference temperature:		70°F
a7.	Radiation loss (assumed):	(5%)	0.05 (5%)
a8.	Excess air rate (EAR)[assumed]		0.885 (i.e., 88.5% XSair)
a9.	Humidity at 60% RH and 80°F	0.0132 kg H_2O/ kg-dry-air	0.0127 lb H_2O/ lb-dry-air
a10.	Standard volume:	24.04 scm/ kg-mole	386.9 scf/lb-mole
a11.	Water latent heat:	2460 kJ/kg	1057 B/lb
	Heat capacity (specific heat):		(where B = Btu)
a12.	Ash	0.83 kJ/kg-C	0.25 B/lb-F
a13.	Flue gas:	1.09 kJ/kg-C	0.26 B/lb-F
a14	Water:	2.35 kJ-kg-C	0.49 B/lb-F

a15. 1kcal/g=	4187	kJ/kg	1799 B/lb
	2.33	kJ/kg	1 B/lb
	1	kJ/kg	0.43 B/lb
	1.06	kJ	1 B
	1	m	3.28 ft
a16. Natural gas (NG): (heat of combustion)	13.3	kcal/g	23932 B/lb

	POHC ratio	waste lb/h	ΔHc kcal/g	B/lb	Mixture B/h
Hexachloroethane, C_2Cl_6	0.0487	58.44	0.46	828	4.84E+04
Tetrachloroethene, C_2Cl_4	0.0503	60.36	1.19	2141	1.29E+05
Chlorobenzene, C_6H_5Cl	0.2952	354.24	6.60	11876	4.21E+06
Toluene, C_7H_8	0.6058	726.96	10.14	18246	1.33E+07
Water, H_2O		0		0	
Waste		0		0	
Fuel		0		0	
		0		0	
	1.0000	1200.00			1.76E+07

Therefore, the heat value of the POHC mixture = 14,667 B/lb

a17. Natural gas (NG): (heat of combustion)	13.3	kcal/g
a18. Total waste heat input:	1.76E+07	B/h

a19. Chemical analysis:

	Σ C's	Σ H's	Σ Cl's	Σ O's	Σ Molecular Weight, M
C_2Cl_6	24.00	0	213	0	237.00

		lb/h
C's/M	0.1013	5.92
H's/M	0.0000	0.00
Cl's/M	0.8987	52.52
O's/M	0.0000	0.00
	1.0000	Σ = 58.44

C_2Cl_4	24.00	0	142	0	166.00
C's/M	0.1446				8.73
H's/M	0.0000				0.00
Cl's/M	0.8554				51.63
O's/M	0.0000				0.00
	1.0000				Σ = 60.36

C_6H_5Cl	72.00	5	35.5	0	112.50
C's/M	0.6400				226.72
H's/M	0.0444				15.74
Cl's/M	0.3156				111.78
O's/M	0.0000				0.00
	1.0000				Σ = 354.24

C_7H_8	84.00	8	0	0	92.00
C's/M	0.9130				663.72
H's/M	0.0870				63.24
Cl's/M	0.0000				0.00
O's/M	0.0000				0.00
	1.0000				Σ = 726.96

Fuel (natural gas, CH_4) to kiln: 1200 scf/h
Fuel density = Molecular Wt/std volume (a10): 0.04135 lb/scf
Fuel weight flow rate = fuel density x fuel volume flow rate
= 49.62 lb/h

CH_4	12.00	4	0	0	16.00
C's/M	0.7500				37.22
H's/M	0.2500				12.40
	1.0000				49.62

H_2O in fuel: 0

a19. Fuel heat input = weight rate x HHV: 1.188+06 Btu/h
a20. Total Heat In = Waste Input (a18) + Fuel Input (a19): 1.88E+07 Btu/h
Total average heating value = a20/(waste + fuel): 15,045 Btu/lb

*****Test data was 15,200 Btu/lb*****

a21. Chemical analysis summary (in lbs/hr):

	W & F analysis	F: fuel	unburned carbon	W: waste feed	total combustible feed	Fraction of combustible feed
C:		37.2		905	942.2	0.7540
H:		12.4		79	91.4	0.0731
Cl:				216	216	0.1729
O_2:				0	0	0.0000
N_2:				0		
S:				0		
H_2O				0		
Ash:				0		
Fly ash: (unburned carbon becomes ash):				0		
		49.6		1200	1249.6	1.0000

b. Theoretical Combustion Air

b1. Calculation of oxygen needs
$C+O_2 \rightarrow CO_2$
$O_2=C*32/12=2.67*C=$ 2.67(942.2)= 2516 lb/hr
H left over after Cl's reaction (HLO)
HLO=H-Cl/35.5= 85.32 lb/hr
$H_2+0.5O_2 \rightarrow H_2O$
O_2=HLO*0.5*32/2= 682
$S+O_2 \rightarrow SO_2$ $O_2=S*32/32$ 0
- Bound O_2 0

b2. Theoretical oxygen (Th. O_2) 3198 99.94 mole/h
b3. Th. nitrogen, $N_2=(Th.O_2)*3.76*28/32$ 10521 375.77 mole/h
b4. Theoretical dry air = Theor. O_2+N_2: 13719 475.71 mole/h

b5. Humidity: 0.0127

b6. Water due to humidity = b4*b5 174

b7. Actual theor. air=dry theor. air+its H_2O 13893

b8. Theor. reactants=actual theor. air+feed 15143 lb/hr

b9. Theoretical air combustion products:
$CO_2=C*44/12$: 3455 lb/hr 78.52 mole/h
$SO_2=S*64/32$ 0 0.00

b10. H_2O=HLO*18/2:	768	42.66
N_2=(Th.O_2)*3.76*28/32	10521	375.77
HCl=Cl*36.5/35.5	222	6.08
b11. H_2O in feed:	0	0.00
Fly ash:	0	0.00
Ash:	0	0.00
b12. H_2O due to humidity:	174	9.67
N_2 with waste:	0	0.00
b13. Theor. combustion products:	15140 lb/hr	513 mole/h
b14. Check (b8=b13):	15143 lb/hr	
b15. Combustion dry gas=CO_2+SO_2+HCl+N_2:	14198 lb-dry-gas/hr	
b16. Combustion gas H_2O: (b10+b11+b12)	942 lb H_2O/hr	
	15140 lb/hr	

c. Actual Combustion Air:

Excess air rate, EAR (a8): 0.885 (assumed)

c1. O_2, additional=EAR*(Th.O_2):	2830
c2. N_2, additional=EAR*(Th.N_2):	9311
c3. Actual Excess dry air:	12141
c4. Excess H_2O (b5xc3):	154 lb/h

c5. Actual dry air= theor. air+Additional O_2 and N_2 25860 lb-dry air/h

c6. H_2O associated with actual air = (b5xc5 or b12+c4): 328 lb H_2O

c7. Actual air=dry air+H_2O in air: 26188 lb-air/h=908 lb-mole/h (c5+c6)

c8. Air flow rate = std. volume (a10) x lb-mole/h=351305 scf/h =(a10 x c7): =5855 scf/min

*****Test data was 3600 cfm*****

Total water vapor in flue gas

• With waste (a21):	0 lb/h
• Due to combustion (b10):	768
• Humidity (c4+b12):	328
• Quenching water:	0

c9. Total water vapor in flue gas = 1096 lb/hr

c10. Actual reactants=actual dry air+feed + H_2O in combustion air (a21+c7)= 27438 lb reactant/hr =27438 lb product/hr

Actual Combustion Products (i.e., Flue Gas):

c11. O_2 leftover in products = 2830 lb/hr
Additional O_2 = c1:
c12. O_2 content in flue gas = 0.1031 = 10.31%
c11 ÷ c10:
**** Test data was 10.3% ****

d. Calculation of Exit Temperature from Kiln

d1. Total heat in=Waste Heat Input (a18) + Fuel Heat Input (a19)=a20: 1.88E+07 B/h
d2. Overall heat loss (assumed as 5%, see a7): 0.0940E+07

Unburned carbon:
d3. Unreleased heat (due to unburned carbon): 0.0000E+00

Trial #1
Assumed exit temp.: 1500°F
Reference temp.: 70°F

d4. Temp. difference (ΔT): 1430°F
d5. Heat in dry flue gas=mCpΔT =[c10-c9)xa13xd4] 0.9794E+07B/h
d6. Heat in water = mCpΔT =(c9xa14xd4): 0.0768E+07
d7. Total latent heat = (c9xa11): 0.1158E+07
d8. Heat in ash = mCpΔT=(a2xa12xd4): 0.0000E+00
d9. Total heat accounted for= (d2+d3+d5+d6+d7+d8): 1.2660E+07

d10. Net heat balance = (a20-d9)=(d1-d9): 0.6140E+07B/h

Trial #2
Assumed exit temp.: 2500°F
Reference temp.: 70°F

d11. Temp. difference (ΔT') 2430°F
d12. Heat in dry flue gas=mCpΔT' =[(c10-c9)xa13xd11]: 1.6643E+07
d13. Heat in water=mCpΔT' =c9xa14xd11): 0.1305E+07
d14. Total latent heat=(c9xa11): 0.1158E+07
d15. Heat in ash=mCpΔT'=(a2xa12xd11): 0.0000E+07
d16. Total heat accounted for=(d2+d12+d13+d14+d15): 2.0046E+07b/h
d17. Net heat balance=(a20-d16): -0.1246E+07b/h

d18. Using the interpolation method to estimate kiln temperature, we have:

x1	1500°F	0.6140E+07 B/Hr	y1	
	x	0.00E+00	y	y=0
x2	2500	-0.1246E+07	y2	

$$(x-x1)/(0-y1)=(x2-x1)/(y2-y1)$$
$$x=x1-y1(x2-x1)/(y2-y1)$$

d19. x= 2331°F

*****Test data was 1800°F (average kiln exit temperature)*****

SUMMARY OF CALCULATED RESULTS AND MEASURED RESULTS

Based on the calculations contained herein and information provided by the trial burn results, a summary of key data are provided in the following Table:

SUMMARY OF CALCULATED AND TRIAL BURN RESULTS

	Calculated Results	Measured Results
• O_2 content in Flue Gas	10.31%	10.3%
• Heating Value	15,045 Btu/lb	15,200 Btu/lb
• Exit Kiln Temperature	2331°F	1800°F (average)
• Air Flow Rate	5855 scfm	3600 cfm

CONCLUSIONS

The above Table shows that the differences between the calculated and the measured results are small with the exception of the kiln exit temperature and the air flow rate. The calculated value of the air flow rate is about 63% greater than the trial burn (measured) value. The difference is due to the fact that the measured air rate values neglected to account for the amount of air in- leakage which has to occur in any actual (negative pressure) kiln combustion operation. The measured data relative to oxygen content shows that the calculated air in the system (the 5855 scfm amount) is reasonable because the oxygen content measured downstream of the kiln matches the calculated oxygen concentration (the 10.3%). The calculation, therefore, confirms that the air needed is much more than the 3600 cfm measured value (which, of course, proves that air in-leakage phenomena does occur). The fact that the measured kiln exit temperature is also much lower (about 530°F lower) than the calculated kiln exit temperature indicates that the assumed amount of heat loss (the 5% figure) is probably too low.

It is hoped that these example calculations will assist those who must design incinerators or those who must know how to evaluate their performance (such as governmental permit writers, consultants and public interest groups).

REFERENCES

(EPA, 9/86), "Permit Writer's Guide Test Burn Data: Hazardous Waste Incineration," EPA/625/6-86/012, September 1986.

(Lee, 6/90), "Review of Mobile Thermal Technologies for Solid Waste Destruction," C.C. Lee, G.L.Huffman and D.A. Oberacker. Presented at the 83rd National Meeting of the Air and Waste Management Association, Pittsburgh, Pennsylvania, June 24-29, 1990.